

<https://doi.org/10.15407/ufm.26.01.151>

V.B. TARELNYK^{1,*}, **O.P. HAPONOVA**^{2,3,**},
N.V. TARELNYK^{1,***}, and **Ye.V. KONOPLIANCHENKO**^{1,****}

¹ Sumy National Agrarian University,
160 Herasyma Kondratieva Str., 40021 Sumy, Ukraine

² Sumy State University,
116 Kharkivska Str., 40007 Sumy, Ukraine

³ Institute of Fundamental Technological Research,
Polish Academy of Sciences,
5B Pawińskiego Str., 02-016 Warsaw, Poland

* tarelnyk@ukr.net, ** gaponova@pmtkm.sumdu.edu.ua,

*** natasha-tarelnik@ukr.net, **** konoplyanchenko@ukr.net

SULPHURIZING OF METAL SURFACES BY ELECTROSPARK-DISCHARGE ALLOYING. Pt. 1: Structural-Phase State of Sulphur-Containing Coatings on Constructional Steels

The methods of surface sulphur saturation of metal surfaces to provide them with special tribotechnical properties are reviewed and analysed. The main attention is focused on technologies based on the method of electrospark alloying (ESA). As shown, the process of sulphur saturation can be realised by using a special sulphur-containing saturating technical substance (STS). The methods of forming sulphided, sulphocarbured, sulphoaluminized, Al-C-S, and sulphomolybdenum coatings on steels using STS by ESA are considered. The results of sulphur distribution in the surface layer during ESA sulphurizing with a metal electrode using STS are presented. As shown, the sulphur concentration on the surface is of about 0.53–0.60% that gradually decreases deeper into the substrate. The topography of the treated surface and its structure after sulphocarbured of steel surfaces with a graphite electrode using STS containing sulphur are investigated. As found, the coating consists of several layers: a ‘soft’ layer saturated with sulphur, a hardened layer saturated with carbon, and the substrate metal.

Citation: V.B. Tarelnyk, O.P. Haponova, N.V. Tarelnyk, and Ye.V. Konoplianchenko, Sulphurizing of Metal Surfaces by Electrospark-Discharge Alloying. Pt. 1: Structural-Phase State of Sulphur-Contain, *Progress in Physics of Metals*, **26**, No. 1: 146–200 (2025)

© Publisher PH “Akademperiodyka” of the NAS of Ukraine, 2025. This is an open access article under the CC BY-ND license (<https://creativecommons.org/licenses/by-nd/4.0>)

The thickness, microhardness, and continuity of the coating increase with the discharge energy. The qualitative parameters of sulphoaluminized coatings obtained by the ESA method with an aluminium electrode using STS are analysed. The microstructures reveal three zones: a near-surface, non-continuous loose layer with sulphur enrichment, 10–100- μm thick, and microhardness of 1368–2073 MPa; a ‘white’ hardened layer containing aluminium, 20–40 μm -thick, and microhardness of 4094–5157 MPa; a diffusion zone; and a substrate material. The sulphoaluminized-coatings’ phase composition depends on the ESA energy parameters. Intermetallics FeAl and FeAl₂ are formed in the surface layer. The structural–phase state and properties of sulphomolybdenum coatings obtained by the ESA method with a molybdenum electrode using STS are discussed. The near-surface loose layer saturated with sulphur contains up to 8% of molybdenum disulphide formed due to ESA. Beneath this layer is a hardened layer saturated with molybdenum and having a microhardness of 10596–10731 MPa. It is proposed to use sulphurizing methods based on ESA using STS as cheap and effective methods of surface modification of friction surfaces to reduce seizure and friction coefficient.

Keywords: sulphurizing, electrospark alloying, coating, microstructure, tribotechnical properties.

1. Background and Formulation of the Problem

Today, technology possesses a very large number of methods for improving the quality of surfaces of machine parts in various industries. Machines operating in agriculture, chemical, oil refining, aerospace, and other fields of industry constantly have been being improved, which entails the need to create more reliable and durable parts and assemblies thereof.

The destruction of a part starts from its surface. Therefore, *i.e.*, to ensure the reliability of a friction pair, an important factor is to improve exactly the quality of the surface layer of the parts in contact. Although the wear of friction surfaces is indeed reduced when using hard wear-resistant and, as a rule, expensive materials [1–3], there is no need to use them to make the entire part. It is enough to provide only the part surface layer with the necessary operational properties, and the ‘core’ (base material) can be made of cheaper materials that still have mechanical strength [4–6].

Developing the new composite materials, which have a hard wear-resistant surface and base of high fatigue strength, is an urgent task [7–10].

The most traditional technologies that provide the surfaces of parts with the necessary physical, chemical, tribological, and operational properties include: applying metal-ceramic coatings onto wear surfaces [11–13], weld overlay cladding of the coatings made of composite materials [14, 15], providing vapour-phase deposition [16], providing physical vapour-phase deposition [17, 18], laser cladding [19], laser melt injecting [20], composite electroplating [21], providing chemical deposition [22]. This also includes centrifugal reinforcement of the steel surface layers with tungsten carbide particles [23], coatings including the layers of aluminium oxide [24–26], and electrochemical spilling solution chromizing [27]. A separate

niche among the technologies used to increase the reliability and durability of the parts by introducing chemical elements into their surface layer is occupied by thermochemical treatment (TCT), which combines carburizing, nitriding, nitrocarburizing and several other methods [28–30].

Sulphurizing, as a method for saturating the surface layer of steel or cast iron with sulphur and for creating a sulphide film, which reduces the processes of seizure and sticking of the contacting surfaces of the parts during friction, is one of the widely used thermochemical methods.

Increasing the performance of cutting tools made of high-speed steels can be achieved by saturating their highly stressed surface layers with elements such as nitrogen, carbon and sulphur using the thermochemical treatment methods [31–33].

As compared to light oils, the most effective way to reduce a machine's part wear is to use a hard lubricant. FeS boundary lubricating film is considered an excellent hard lubricant due to its hexagonal structure, low shear, strength and high melting point. In addition, its cost is very low. It is equal to about 1% of MoS₂ cost [34–36].

FeS lubricating coatings applied to steel by ionic sulphonation [34, 37–39], plasma spraying [34, 40], or ionic sulphonation with a plasma source [41] can significantly improve the wear resistance of parts.

To improve a machine-part surface quality, the technologies that apply for processing the concentrated energy flows (CEFs) are increasingly being used. While applying the CEF technologies, it is possible to form heterogeneous surfaces that differ in geometry, hardness, chemical and physical properties. Such surfaces can be obtained by various methods, *i.e.*, plasma spraying [42–44] and plasma treatment [45, 46], laser processing, and applying electrospark coatings (EC) with the use of the electrospark alloying (ESA) method [47–49].

The properties of a surface layer formed by the ESA method differ from the properties of the base material [50–52]. The quality of the surface layer formed by the ESA method can be improved by a subsequent laser processing method [53–56].

Owing to the ESA method, in the surface layers, there are formed surface structures having unique physical-mechanical and tribological properties at the nanolevel [57–59].

In the course of processing with the use of the ESA method, the surfaces of the electrodes (anode and cathode) are locally exposed to high shock wave pressure and temperature [60, 61]. The temperature of a short-term heating of the surface in a local place can reach $(5-7) \times 10^3$ K. The spark discharge occurs in small volumes and lasts 50 to 400 microseconds. In the cathode, there are formed tiny indentations (microbaths) wherein the particles of the anode and the cathode come into contact with each other and the environment. This event contributes to the creation of new phases and changes in the structure of the surface layer.

The advantages of the ESA technology, which distinguish it from other methods of surface treatment, are the environmental safety, the impact in local places, the high adhesion, the absence of changes in the geometric shape of the part, *etc.* [62, 63].

Such possible disadvantages of the ESA method as increased roughness and lack of continuity of the applied coating, surface porosity [64, 65], and insignificant thickness of coatings often become its advantages. For example, special preliminarily roughening (creating surface roughness) [66] before applying metal-polymer materials (MPM) or spraying provides for better adhesion of the applied materials to the substrate.

With the so-called 'finishing' ESA method, it is possible to obtain the high-quality and wear-resistant coating (of 100% continuity and a thickness of up to 1.0 mm and even more), *i.e.*, when restoring the surfaces of screw compressor bands [67]. The availability of pores in the coating helps to retain a layer of lubricant, *i.e.*, in shaft-bearing journals [68, 69].

As noted above, among chemical treatment technologies, there is widely used a method of sulphurizing, namely, a thermochemical process for treating the parts made of iron-based alloys to saturate their surfaces with sulphur. The sulphide film has strength lower than the base metal, so it is easily destroyed by friction, preventing seizure of friction surfaces [70].

The sulphurizing traditionally takes place in the appropriate salt baths. In this case, the surface roughness increases and the dimensions of the parts slightly grow in size [71]. In addition, the entire part is heated up and, as a result, there occur the changes in the structure of the metal, deformations and warping events. The process lasts up to three or more hours. There is observed high-energy consumption and negative impact on the environment, *etc.*

In Ref. [72], the authors carry out sulphurizing with the use of the ESA method. In this case, to introduce sulphur into the part surface, it is applied in the form of a powdery layer onto the area being alloyed. In other words, the area is 'powdered', and the process is repeated two or three times.

It should be noted that this method could not always provide for the desired result, because sulphur is a dielectric, which makes it difficult for it to enter the microbath of molten metal and create chemical compounds. This process becomes much more complicated and occurs in separate isolated areas. Formed on the surface, the sulphide film has a low continuity.

According to Ref. [73], the authors carried out the ESA process for applying iron sulphide on steel 45, steel X12Φ (Kh12F), grey, and pearlite ductile cast iron. At the same time, a sulphur-enriched layer having a thickness of 40–50 microns was formed on the alloyed surface. This event significantly reduced the tendency of grey cast iron to scuff during dry friction. In this case, the wear was reduced by up to 10 times.

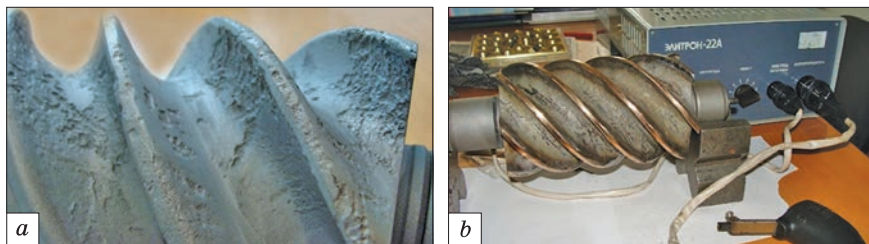


Fig. 1. Screw compressor (SC) rotor before (a) and after (b) restoring the outside surfaces of the edges of the teeth with the use of the bronze electrode [75]

In the course of the ESA process, the use of iron sulphide as an electrode instrument (EI) to carry out the process of sulphurizing has several disadvantages:

- first, this is the limited use of unalloyed steel (iron) electrodes;
- during ESA processing, the electrodes are heated, oxidized and destroyed, which negatively affects the quality of the formed coating (high roughness, low continuity, welding of individual small particles from the destroyed anode);
- such EIs may not be used in mechanical facilities due to their burnout;
- an expensive and labour-intensive method for producing the EIs.

In work [74], to eliminate the above-described shortcomings, a new method for producing the EIs for carrying out the sulphurizing process by the ESA method was proposed. In the event, as EI materials, there could be used such pure corrosion-resistant metals as chromium, nickel, molybdenum, and others, such stainless steels as 12X18H10T (12Kh18N10T), 07X16H6 (07Kh16N6), 30X13 (30Kh13), and others; and such nickel alloys as XH58МБУД (KhN58MBUD), XH60BT (KhN60VT), XH50BMTYB (KhN50VMTUB), *etc.*

A process for repairing a screw compressor (SC) rotor is described in Ref. [75]. A machine with a manual vibrator model 'ELITRON-52A' was used to restore the outer surfaces of the tooth edges. O10I1.5H (O10Ts1.5N) bronze was used as the EI in Fig. 1.

The SC rotors are made of structural, high-quality medium carbon steels, namely, steel 40, steel 45, chromium steel 40X (40Kh), *etc.* To reduce such negative factors as seizure, sticking, *etc.* of the rotor surfaces at touching thereof, the hardness of the rotors after the final heat treatment is provided low and makes up of 156 to 217 *HB* for various strength grades.

The SC rotor bands are restored using special EI intended for sulphurizing. In the event of significant wear of the rotor bands (1.0 mm per a diameter or more), such mechanical ESA units as the ones of 'Elitron 347', 'EIL-9' models and others based on screw cutting engine lathes are used to restore them. When that is the case, to restore the worn surfaces

of the rotor band, it is recommended to use a combined technology consisting of the ESA process using the steel EI, which is followed by applying the coatings of metal-polymer materials (MPM) having a good adhesion to the metal, deformation characteristics close to metal, slight changes in properties due to changes in temperature, minimal coating shrinkage, resistance to external factors, *etc.* [76].

To prevent the possibility of scuffing on the steel surface of the restored rotor band, it is restored with the use of the EI made of steel 12X18H10T (12Kh18N10T) containing sulphur. As a result, after the mechanical operation, the surface of the band would consist of separate metal sections containing sulphur and areas made of MPM. At the same time, as the depth of treatment increases, the area of the surface areas of MPM will decrease, and formed by the ESA method, the sulphurized zones will correspondingly increase.

An analysis of relevant literature and patent sources, as well as several studies conducted by the authors of this paper, has shown the promise of work aimed at improving the technology for sulphurizing with the use of the ESA method.

Thus, the available information on phase and structural transformations in the surface layers of steels and various metals during the ESA process by the sulphur-containing EI, the data on the correlation dependencies between the parameters of the ESA process and structural changes in metal surfaces determine the need for analysing of the accumulated experience, systematizing the literary and patent sources in this field, and setting the goals for subsequent research.

The purpose of this work is to analyse the influence of the electric spark alloying parameters (discharge energy and alloying productivity) during sulphurizing on the microstructure and quality of the surface layer (surface roughness, continuity and microhardness of the coating).

2. Research Methodology

To determine the influence of the ESA equipment energy parameters on the quality parameters of the coatings, there were provided the specimens made of steel 20 and steel 40 each having a size of $15 \times 15 \times 8$ mm, whereon the EI coatings were applied on different modes using the 'Elitron 52A' model unit. Each ESA mode corresponded to its own discharge energy and productivity (the area of the formed coating per unit of time in Table 1.

When implementing the sulphurizing process (utility model patents Nos. 115059 UA, 117528 UA and 119317 UA), the electrode-instrument workpiece in the form of a wire, rod, *etc.*) was provided with indentations using any known method (punching, drawing through a die, threading, *etc.*).

Figure 2, *a* shows the EI made of stainless steel 12X18H10T (12Kh18N10T) \varnothing 3 mm, on which the thread is applied. Sulphur, *i.e.*, in the

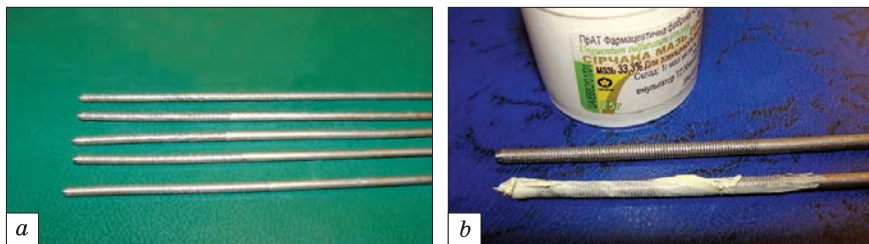


Fig. 2. EI made of stainless steel 12X18H10T (12Kh18N10T) 3 mm, intended for sulphurizing the parts with the use of the ESA method [74]

form of a sulphur ointment with sulphur content of 33.3%, is applied into the thread indentations in Fig. 2, b. The amount of sulphur can be increased by adding it to the ointment, *i.e.*, in the form of colloidal sulphur. After removing excess sulphur and drying, the electrodes are ready for use.

To saturate the surface of the specimen with sulphur, the coating was applied by the ESA method with the use of the special EI made of stainless steel 12X18H10T (12Kh18N10T) at the unit of ‘Elitron 52A’ model with $W_p = 0.55$ J.

The EI of 30–35 mm length was made of a \varnothing 3 mm wire of 12X18H10T (12Kh18N10T) steel by cutting the M3 thread on the length of 25 mm. The indentations obtained on the surface of the electrode were filled with a special technological (technical) substance (STS), namely, sulphur ointment, wherein the concentration of sulphur was 33.3%. The excess of the STS was removed with a napkin.

At sulphocarburing (invention patents No. 2663799 RU, utility model patent No. 117867 UA, 119318 UA), immediately before alloying with a graphite electrode, a special technological substance (STS), namely, a consistent substance containing sulphur, was applied onto the surface of the steel part. As a consistent substance, sulphur paste and/or sulphur ointment were used. The amount of sulphur in the consistent substance was increased by adding colloidal sulphur thereto. The ESA process was carried out at the Elytron-52A model unit at $W_p = 0.13$ –3.4 J. Applying the STS to the surface of the steel part immediately before alloying with the use of the graphite electrode allows obtaining the steel parts having an increased fitting and high wear resistance.

At sulphoalizing (invention patents Nos. 121343 UA and 2696616 RU, utility model patent No. 130157 UA), the specimens having a size of 15×15×8 mm each were made of steel 20 and steel 40. The specimens being

Table 1. Dependence of ESA productivity on discharge energy [74]

Discharge energy W_p , J	0.52	1.3	2.6	4.6	6.8
Productivity, cm ² /min	1.0–1.3	1.3–1.5	1.5–2.0	2.0–2.5	2.5–3.0

investigated were applied with a special STS, namely, the consistent substance in the form of sulphur ointment with a sulphur content of 33.3%. Before applying, the ПАД-0 (ГОСТ 5494-95) [PAD-0 (GOST 5494-95)] aluminium powder was added to the STS. The powder maximum amount was 56%. A further increase in the powder amount resulted in decreasing adhesion with the surface being aluminized. After that, without waiting for the STS to dry, the ESA process was performed applying different modes with the use of an aluminium electrode.

The rods of \varnothing 4 and 45 mm long made of СВА99 (ГОСТ 7871-75) [SvA99 (GOST 7871-75)] aluminium wire were used as the EI.

At applying the Al + C + S combined coating was applied (invention patents Nos. 121346 UA and 2707776 RU, utility model patent No. 130866 UA), the specimens were made of steel 20 and steel 40. The specimens being investigated were applied with a special STS composition consisting of a sulphur ointment having a 33.3% sulphur content and a 56% content of ПАД-0 (ГОСТ 5494-95) [PAD-0 (GOST 5494-95)] aluminium powder. After that, without waiting for drying of the consistent substance, the ESA process was carried out with the use of graphite EI on different modes and at corresponding productivity.

It should be noted that a decrease in the productivity of the ESA process leads to a decrease in the quality parameters of the surface layer, namely, the appearance of burns, and most importantly, the destruction of the formed layer, which is especially evident on the heavy-duty modes at the discharge energies of $W_p > 1$ J.

An increase in productivity leads to a decrease in the continuity of the coating. To study the effect of carbon on the properties of the coating being formed, the alloying process of the consistent substance of the composition described above was carried out with ЭГ-4 (EG-4) graphite electrode.

At applying the Mo + S combined coating (invention patent UA No. 144932), the specimens were made of steel 20 and steel 40 (ГОСТ 1050-88 (GOST 1050-88)). The specimens being investigated were applied with a special STS composition consisting of a sulphur ointment with the addition of colloidal sulphur. Without waiting for the STS to dry, the ESA process was carried out with the use of an electrode made of molybdenum at the discharge energy of $W_p = 0.13-3.4$ J and productivity from 0.8 to 2.5 cm²/min. As EI, a molybdenum rod having a diameter of 4 mm and a length of 45 mm was used.

At all the stages of processing, the surface roughness was determined using a profilograph-profilometer device of 201 model of the Kalibr plant production. While determining, the results were being displayed onto the monitor through a special device.

The investigations of the macro-and microstructural parameters of the electrode materials were carried out using the optical microscopes of MIM-7, Neofot-2 models, the REMM-102 raster electron microscope, the

scanning electron microscope of Jeol JSM-5400 model equipped with the microanalyser of ISIS 300 Oxford instruments production, the scanning electron microscope of SEO-SEM Inspect S50-B model equipped with the AZtecOne energy dispersive spectrometer with the X-MaxN20 detector manufactured by Oxford Instruments plc.

Providing metallographic sections, preparing surfaces, and metallographic studies were performed according to the known methods [77]. A 3–5% solution of nitric acid in ethyl alcohol was used as a reagent for chemical etching of steel 20, steel 40, 38X2MIOA (38Kh2MJuA) steel, and cast iron. For the steels of 30X13 (30Kh13) and 12X18H10T (12Kh18N10T) grades, the reagent aqua-regia was used.

The durometric studies of the layer components were performed using the PMT-3 microhardness tester by indenting a diamond pyramid under a load of 0.05 N [78, 79]. The microhardness was determined as the arithmetic mean value of the measurements of the diagonals of the prints without visible cracks and shearing distortions.

The continuity of the coating was determined using the L method [80, 81] according to the formula:

$$S = \frac{b \sum a_i m_i}{l},$$

where b is the eyepiece scale division (μm), a_i is the average values of inclusion sizes (μm), m_i is the number of inclusions of the group, and l is the defined length (μm).

The x-ray studies were performed in CuK_α and CoK_α radiation using the DRON-3 and AXRD Benchtop diffractometers produced by Proto Manufacturing Inc., the USA. The diffractograms were taken by step-by-step scanning. The scanning step was 0.050; the exposure time at a point was of 3 s.

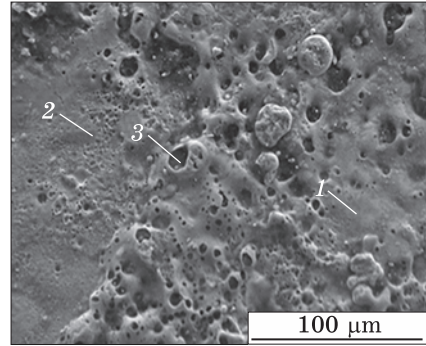
To determine the elemental composition of the coating, the qualitative and quantitative local analyses were carried out. For this, there were used such microscopes as the raster microscope REMM-102, equipped with an attachment including an x-ray microanalyser, the Jeol JSM-5400 scanning electron microscope, equipped with an ISIS 300 Oxford Instruments microanalyser, the SEO-SEM Inspect S50-B scanning electron microscope, equipped with the AZtecOne energy dispersive spectrometer with an X-MaxN20 detector manufactured by the Oxford Instruments plc).

3. Results and Discussion

3.1. Analysis of the Surface Layer Quality after Sulphurizing [82, 83]

Figure 3 shows the topography of the formed layer surface with three selected characteristic areas (1 — smooth surface, 2 — rough surface, 3 — pore). In Figure 4 and Table 2, there is shown a spectrum of the surface and an elemental composition both for the characteristic points and for

Fig. 3. Topography of the steel 20 surface section after sulphurizing by the ESA method [82, 83]



the entire surface being studied, respectively. The distribution of the elements along the depth from the surface at the scanning step of 15 μm (according to Fig. 5) is in Table. 3.

Table 4 shows the results of sulphurizing the specimens made of steel 20 and ВЧ60 (VCh60) high-strength cast iron using a special electrode made of 12X18H10T (12Kh18N10T) stainless steel. The electrode had been manufactured according to the proposed method.

Thus, at saturating the surface of steel 20 with sulphur by the ESA method with the use of a special tool electrode made of 1218H10T (12Kh18N10T) stainless steel at the Елітрон-22А (Elitron-22A) model unit with the discharge energy $W_p = 0.55$ J, the concentration of sulphur on the surface was of 0.53–0.60%. While deepening, the concentration of sulphur had been decreasing gradually, and at a depth of 75 μm, it was about 0.06%.

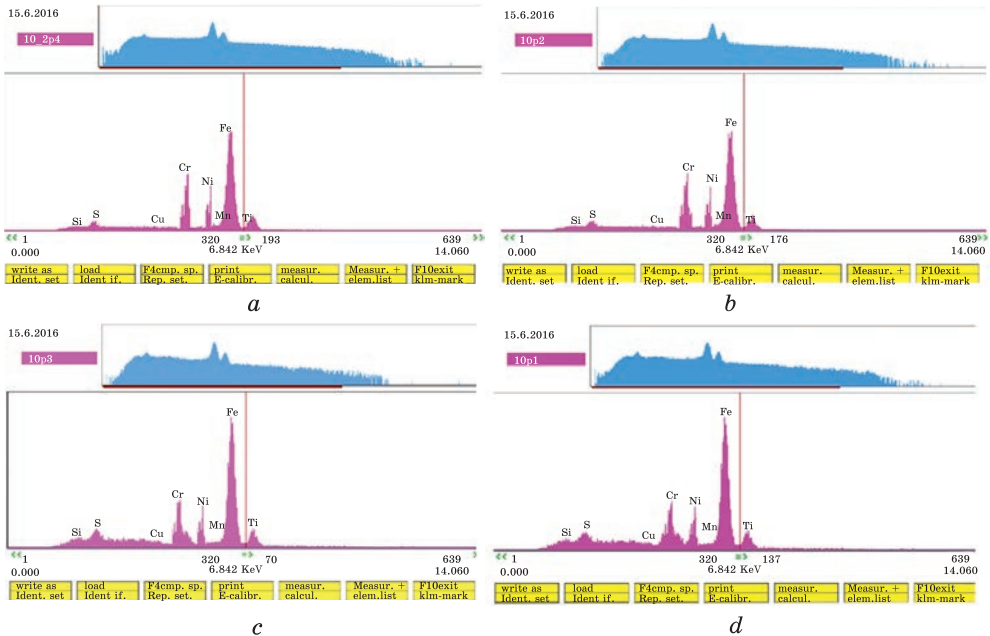


Fig. 4. Spectra from the coating surface: 1 — smooth surface, 2 — rough surface, 3 — pore; (a) smooth surface, (b) rough surface, (c) pore, (d) the entire surface [83]

Table 2. Elemental composition both for the characteristic points and for the entire surface being studied [83]

Point being studied, surface area (Σ)	Elements, %							
	S	Cu	Si	Mn	Cr	Ni	Ti	Fe
1	0.56	0.20	0.24	0.60	16.20	9.30	0.71	72.16
2	0.60	0.21	0.22	0.58	17.21	8.89	0.69	71.60
3	0.53	0.23	0.18	0.62	15.23	9.19	0.83	73.19
Σ	0.55	0.87	0.21	0.60	16.87	9.07	0.89	70.94

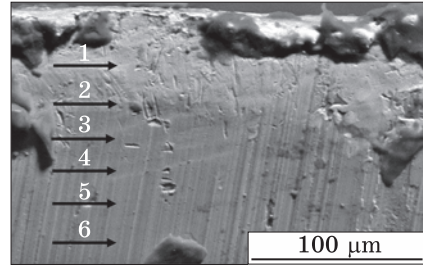
Table 3. Elemental composition of the coating as it deepens from the surface [83]

The surface point being studied	Elements, %							
	S	Cu	Si	Mn	Cr	Ni	Ti	Fe
1	0.41	0.23	0.24	0.58	9.21	5.21	0.61	83.51
2	0.31	0.19	0.22	0.51	5.23	3.19	0.34	90.01
3	0.12	0.20	0.21	0.62	3.19	2.23	0.21	93.22
4	0.09	0.21	0.23	0.57	1.16	1.21	0.17	96.36
5	0.06	0.16	0.16	0.54	0.53	0.76	–	97.79
6	0.03	0.24	0.17	0.53	0.21	0.25	–	98.57

Table 4. The results of sulphurizing the specimens made of steel 20 and high-strength cast iron BЧ60 (VCh60) [82, 83]. Here, one star (*) denotes sulphur content in the lower part of the sulphurized layer, while two stars () denote sulphur content on the surface of the sulphurized layer**

Specimen material	Discharge energy, W_p , J	Sulphurized layer depth, μm	Sulphur content, %	Surface roughness, R_a , μm
Steel 20	0.02	10	0.05*–0.85**	0.7
	0.05	25	0.05–0.80	1.7
	0.11	35	0.05–0.70	2.9
	0.36	50	0.05–0.65	5.2
	0.55	75	0.06–0.60	6.2
	0.90	90	0.06–0.50	7.9
	1.70	100	0.06–0.40	13.7
High-strength cast iron BЧ60 (VCh60)	0.02	10	0.05–0.85	0.8
	0.05	30	0.04–0.70	1.9
	0.11	40	0.05–0.65	3.1
	0.36	50	0.05–0.60	5.8
	0.55	75	0.05–0.50	6.7
	0.90	90	0.04–0.45	8.4
	1.70	100	0.05–0.40	14.6

Fig. 5. Scanning points of the coating elemental composition along the depth of the layer [83]



The list of the alloying elements of the electrode, namely, the electrode — tool made of steel 12X18H10T (12Kh18N10T), comprising Cr, Ni, and Ti, while deepening, gradually decreasing, respectively, from 16.9, 9, and 0.9% on the surface to 1.2, 1.2, and 0.2% at a depth of 60 μm .

Given the fact that the sulphurizing method is used to eliminate the process of seizure the parts in the friction pairs, to reduce their surface roughness, it is expedient to apply:

- the method of non-abrasive ultrasonic finishing in the course of sulphurizing at the discharge energy of $W_p < 0.55 \text{ J}$;
- the grinding method in the course of sulphurizing at the discharge energy of $W_p = 0.55\text{--}1.7 \text{ J}$. In this event, the thickness of the sulphurized layer would decrease by 50 μm .

3.2. Analysis of the Sulphocarbureted Coating Quality [84–88]

To improve hardness and wear resistance, as well as to ensure special tribological properties of the part surfaces, the creation of the sulphocarbureted coatings by the ESA method should be chosen as one of the promising directions.

Figure 6 represents the profilograms of the surface layers formed during sulphocarbureting by the ESA method at $W_p = 0.13, 0.55,$ and 3.4 J on steel 20. As the discharge energy increases, the surface roughness increases too, as shown in Table 5. Thus, at sulphocarbureting by the ESA method with $W_p = 0.13 \text{ J}$, $R_a = 1.1 \mu\text{m}$, and with $W_p = 3.4 \text{ J}$, $R_a = 2.5 \mu\text{m}$.

Figure 7 shows the microstructures of the specimens made of steel 20 after sulphocarbureting on different ESA modes. The conducted metallographic analysis showed that the white layer, which was characteristic of the electrospark coatings, was not pronounced. There was clearly observed

Table 5. Qualitative parameters of sulphocarbureted coatings obtained by the ESA method on steel 20 [84–86]

Discharge energy, $W_p, \text{ J}$	Roughness, μm			Layer of reduced microhardness			Strengthened layer			Amount of sulphur on surface, %	Depth of layer with high sulphur content, μm
	R_a	R_z	R_{max}	$H_{\mu}, \text{ MPa}$	$h, \mu\text{m}$	$S, \%$	$H_{\mu}, \text{ MPa}$	$h, \mu\text{m}$	$S, \%$		
0.13	1.1	2.6	7.1	1350	15	80	1830	30		1.01	60
0.55	1.7	4.6	13.0	1460	20	95	2000	40	100	0.65	90
3.40	2.5	3.9	15.4	1600	30	100	2150	50		0.45	150

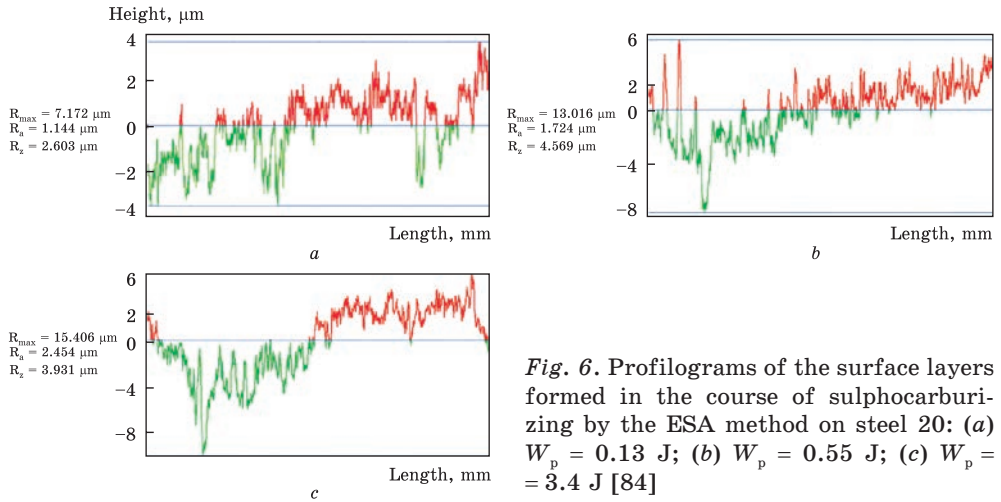


Fig. 6. Profilograms of the surface layers formed in the course of sulphocarburi- zing by the ESA method on steel 20: (a) $W_p = 0.13 \text{ J}$; (b) $W_p = 0.55 \text{ J}$; (c) $W_p = 3.4 \text{ J}$ [84]

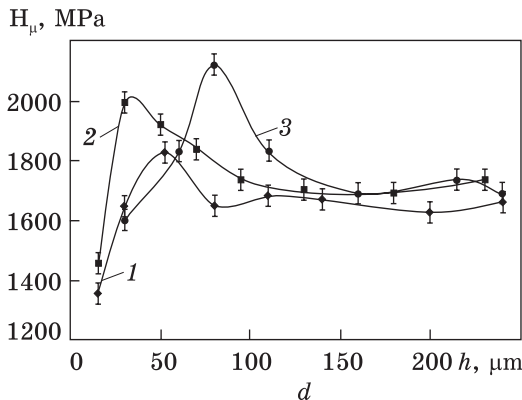
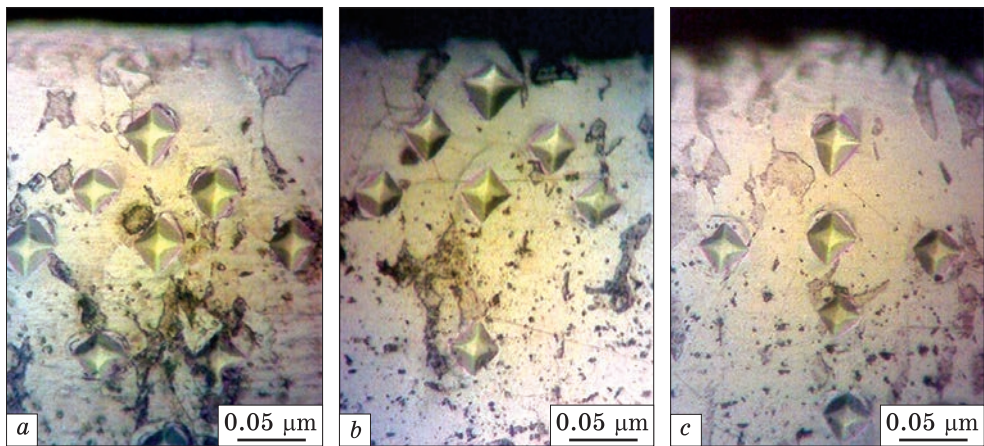


Fig. 7. Microstructure (a–c) and distribution of microhardness (d) in the surface layer of steel 20 after sulphocarburi- zing by the ESA method: (a) $W_p = 0.13 \text{ J}$; (b) $W_p = 0.55 \text{ J}$; (c) $W_p = 3.4 \text{ J}$; (d) On the graph 1 — $W_p = 0.13 \text{ J}$, 2 — $W_p = 0.55 \text{ J}$, 3 — $W_p = 3.4 \text{ J}$ [84]

a diffusion zone, the thickness of which had been increasing with increasing the discharge energy. In the course of the ESA process, due to heating at the intercritical temperature interval for steel 20 (724–845 °C), an incomplete phase recrystallization area had been formed in the diffusion zone.

The durometric studies of the sulphocarbureted coatings indicated that there were two zones, which had been formed in the surface layer, namely, in the near-surface layer, there was a zone of reduced microhardness, and next to that zone of increased microhardness, and there was a strengthened layer, as shown in Fig. 7 and Table 5.

It should be noted that while increasing the discharge energy, the hardness and the depth of the reduced microhardness layer and the strengthened layer had been increasing. Such a feature of the formation of the sulphocarbureted layer obtained by the ESA method was associated with the different indices of diffusion for carbon and sulphur deep down into the metal [86, 89, 90].

Figure 8 shows the topographies of the various areas of the surface layers during sulphocarbureting steel 20 formed, respectively, with the discharge energy of $W_p = 0.13, 0.55, \text{ and } 3.4 \text{ J}$. To evaluate the chemical composition on the surface, the three characteristic zones were chosen: 1 — the smooth surface, 2 — the rough surface, 3 — the pore.

Table 6. The chemical composition of the surface of steel 20 in characteristic zones and from the entire surface was investigated after sulphocarbureting by the ESA method [86]. Here, 1 — smooth surface, 2 — rough surface, 3 — pore, Σ — the entire surface

Point being studied, area (Σ) of the surface	Elements, %						
	S	Cu	Cr	Ni	Mn	Si	Fe
$W_p = 0.13 \text{ J}$							
1	0.97	0.23	0.20	0.21	0.60	0.24	97.55
2	1.2	0.23	0.24	0.19	0.58	0.22	97.34
3	0.87	0.21	0.19	0.16	0.62	0.18	97.77
Σ	1.01	0.22	0.21	0.19	0.60	0.21	97.56
$W_p = 0.55 \text{ J}$							
1	0.77	0.20	0.21	0.21	0.61	0.24	97.76
2	0.64	0.22	0.23	0.17	0.59	0.22	97.93
3	0.53	0.24	0.19	0.14	0.56	0.23	98.11
Σ	0.65	0.22	0.21	0.17	0.59	0.23	97.93
$W_p = 3.4 \text{ J}$							
1	0.57	0.25	0.21	0.19	0.56	0.26	97.96
2	0.34	0.23	0.22	0.17	0.57	0.24	98.23
3	0.53	0.20	0.23	0.15	0.57	0.22	98.10
Σ	0.45	0.27	0.26	0.15	0.59	0.25	98.03

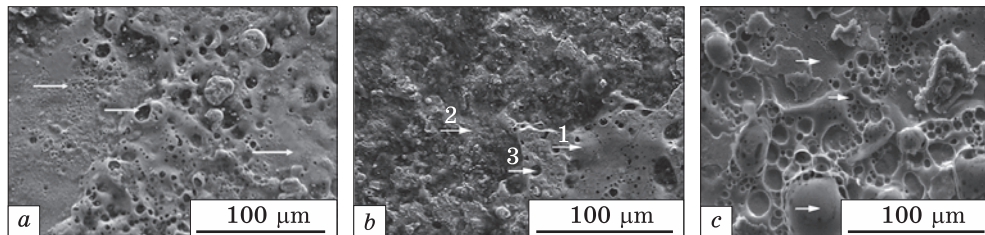


Fig. 8. The topographies of the steel 20 surface areas after the sulphocarburing process: (a) $W_p = 0.13$ J; (b) $W_p = 0.55$ J; (c) $W_p = 3.4$ J [86]

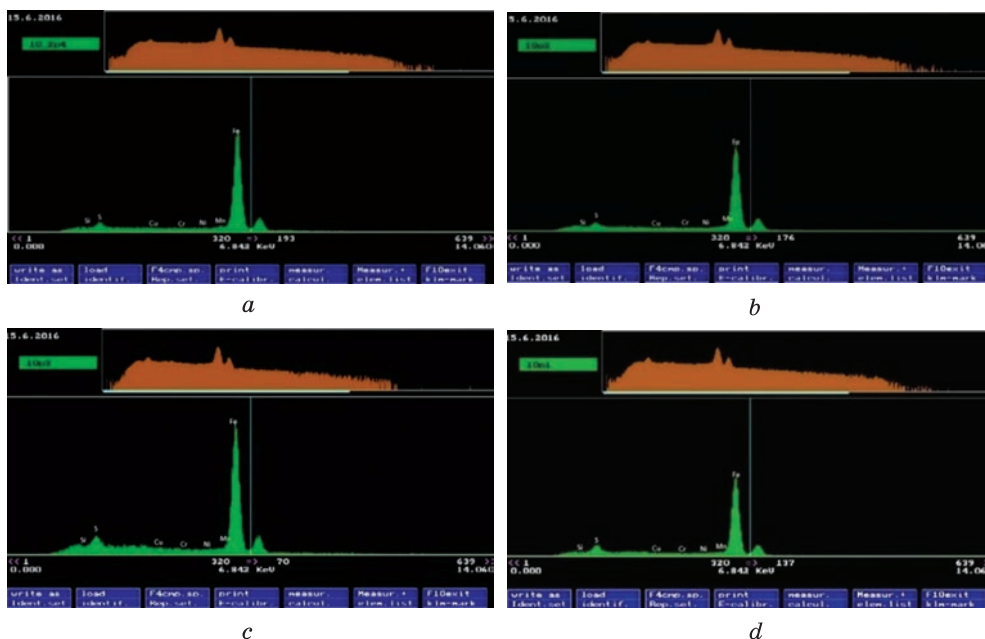


Fig. 9. The spectra from the sulphocarbured surface, $W_p = 0.13$ J: (a) smooth surface, (b) rough surface, (c) pore, (d) from the entire surface [86]

The spectra of the characteristic zones of the sulphocarbured surface at $W_p = 0.13$ J, as well as the chemical composition of the characteristic zones of the formed coatings obtained on the different ESA modes are shown in Fig. 9 and in Table 6, respectively.

Because of the analysis of Table 6, it was found that with an increase in the discharge energy, in all the characteristic zones, a decrease for sulphur was observed. This event is obviously related to the burning of sulphur in the course of providing for the flow of a pulsed discharge in the ESA process. In addition, the increased content of sulphur was found in places of pores, which was explained by the accumulation of sulphur-containing substances in those areas.

Table 7. Distribution of the chemical composition of the steel 20 surface layer in the cross-section after sulphocarburing process [86]

The surface point being studied	Elements, %						
	S	Cu	Cr	Ni	Mn	Si	Fe
$W_p = 0.13 \text{ J}$							
1	0.78	0.21	0.23	0.21	0.62	0.23	97.72
2	0.58	0.19	0.20	0.18	0.59	0.22	98.04
3	0.17	0.21	0.19	0.16	0.62	0.20	98.45
4	0.05	0.22	0.11	0.19	0.61	0.19	98.63
5	0.03	0.18	0.24	0.23	0.59	0.24	98.49
6	0.02	0.20	0.23	0.16	0.63	0.23	98.53
$W_p = 0.55 \text{ J}$							
1	0.54	0.23	0.21	0.21	0.57	0.24	98.00
2	0.41	0.19	0.23	0.19	0.59	0.22	98.17
3	0.25	0.16	0.19	0.23	0.61	0.20	98.36
4	0.12	0.21	0.16	0.21	0.54	0.23	98.53
5	0.08	0.18	0.23	0.16	0.53	0.24	98.58
6	0.05	0.24	0.21	0.25	0.52	0.17	98.56
7	0.03	0.22	0.24	0.19	0.58	0.24	98.50
$W_p = 3.4 \text{ J}$							
1	0.47	0.22	0.24	0.21	0.56	0.23	98.07
2	0.39	0.19	0.23	0.19	0.59	0.22	98.17
3	0.28	0.17	0.18	0.23	0.51	0.20	98.43
4	0.18	0.22	0.17	0.21	0.55	0.23	98.44
5	0.12	0.19	0.24	0.15	0.55	0.23	98.52
6	0.08	0.24	0.21	0.25	0.52	0.17	98.56
7	0.08	0.25	0.23	0.19	0.56	0.23	98.46
8	0.07	0.23	0.20	0.20	0.53	0.25	98.52
9	0.06	0.25	0.21	0.26	0.50	0.20	98.52
10	0.05	0.19	0.20	0.16	0.55	0.23	98.55
11	0.03	0.20	0.19	0.14	0.40	0.23	98.81

Table 8. Qualitative parameters of sulphocarbured coatings obtained by the ESA method on steel 40 [88]

Discharge energy, W_p , J	Roughness, μm			Layer of reduced microhardness			Strengthened layer			Amount of sulphur on surface, %	Depth of layer with high sulphur content, μm
	R_n	R_z	R_{max}	H_{μ} , MPa	h , μm	S, %	H_{μ} , MPa	h , μm	S, %		
0.13	0.97	2.15	6.77	1650	5	70	7074	15	100	1.22	10
0.27	1.44	2.87	8.10	1750	9	85	9374	25		0.95	25
0.52	2.22	3.37	14.08	1900	14	95	13065	40		0.68	40

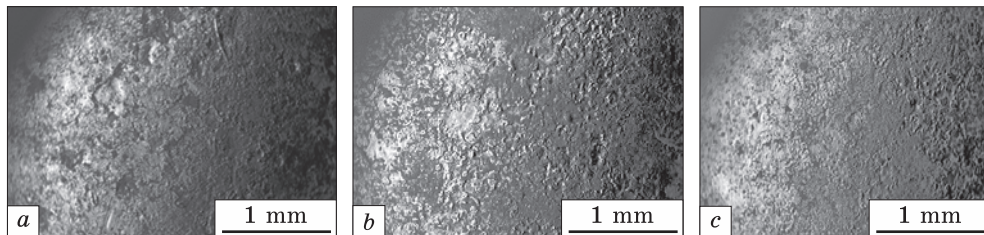


Fig. 10. Topography of steel 40 surface areas after sulphocarburing by the ESA method: (a) $W_p = 0.13$ J; (b) $W_p = 0.27$ J; (c) $W_p = 0.52$ J [88]

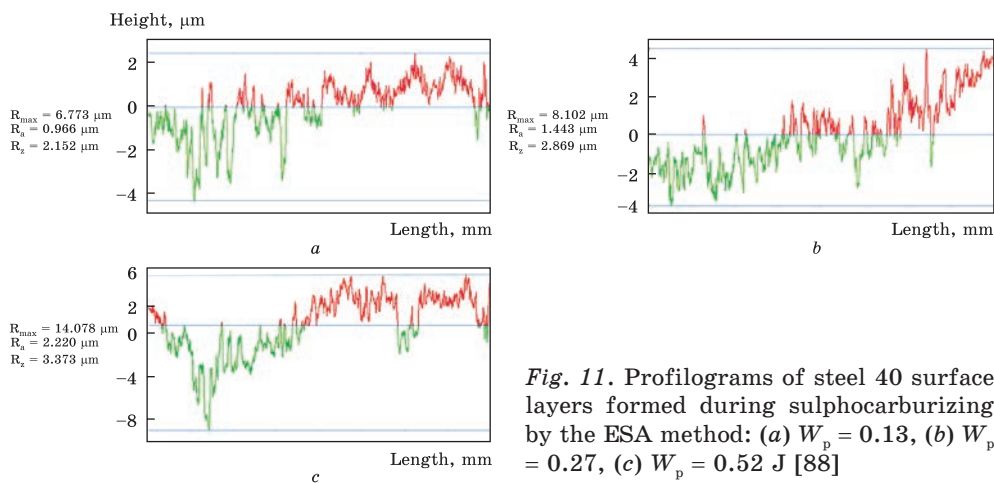


Fig. 11. Profilograms of steel 40 surface layers formed during sulphocarburing by the ESA method: (a) $W_p = 0.13$, (b) $W_p = 0.27$, (c) $W_p = 0.52$ J [88]

There was studied a distribution of the elements in the cross-section from the surface to the base at the scanning step of 15 μm . The results are represented in Table 7.

With an increase in the discharge energy of 0.13 to 3.4 J at ESA processing the steel 20, the amount of sulphur on the surface of the coating has been decreasing. This is, obviously, due to burning sulphur from the surface in the course of passing electric spark discharge. However, due to the intensification of diffusion during the ESA process, at the discharge energy of 3.4 J, the thickness of the sulphurized layer has been increasing in Table 8.

The results of the x-ray spectral analysis indicated that sulphur had accumulated on the surface of the metal at a depth of up to 30 μm . Its concentration at this distance was about 0.4% seen in Table 7. During the ESA process with a graphite electrode, carbon has been diffusing deep into the metal, and at a distance of 30 to 50 microns from the surface, a hardened layer having a microhardness of about 2000 MPa has been formed.

The influence of the sulphocarburing process by the ESA method on the quality parameters of the obtained coatings on the steel 40 specimens has been studied.

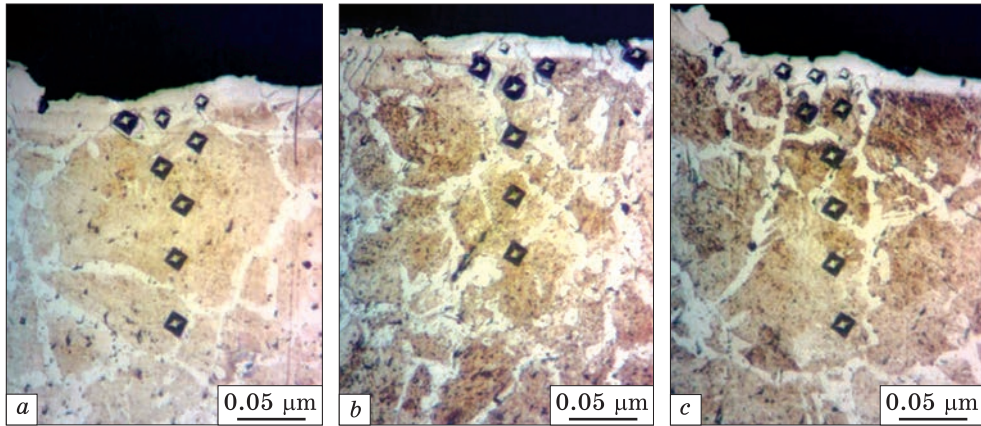


Fig. 12. Microstructure (a-c) and distribution of microhardness (d) in steel 40 surface layer after sulphocarburing by the ESA method: (a) $W_p = 0.13$ J; (b) $W_p = 0.27$ J; (c) $W_p = 0.52$ J; (d) 1 — $W_p = 0.13$ J, 2 — $W_p = 0.27$ J, 3 — $W_p = 0.52$ J

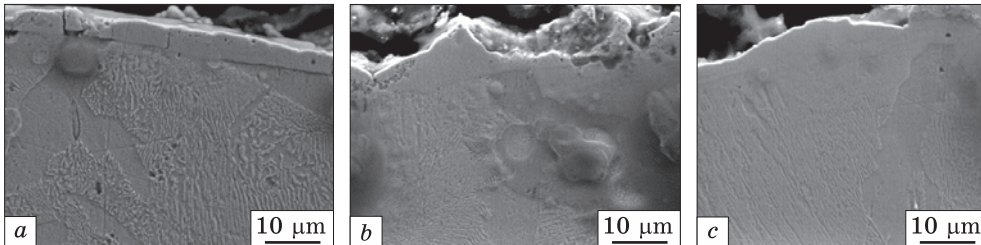


Fig. 13. Results of electron microscopic studies of sulphocarbured on steel 40 layers obtained by the ESA method: (a) $W_p = 0.13$ J; (b) $W_p = 0.27$ J; (c) $W_p = 0.52$ J [85]

Figure 10 represents the topographies of the steel 40 specimen surfaces after sulphocarburing by the ESA method. On analysing the topography of the surfaces of the specimens being studied, it could be concluded that the general natures of the element shapes of the surface micro-roughness were uniform.

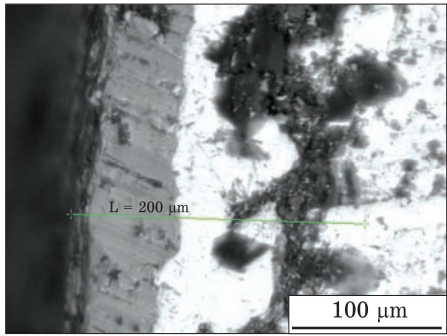
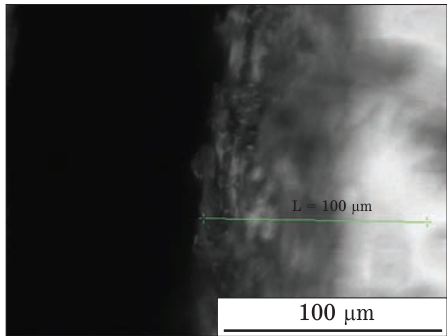
A significant increase in the surface micro-roughness of the specimens was observed after the ESA process at $W_p = 0.52$ J. This is associated with an increase in energy impact. The values of the surface roughness depen-

ding on the energy processing parameters are presented in Table 8, and the profilograms are shown in Fig. 11.

The conducted metallographic analysis of electrospark sulphocarburi- zed coatings using optical and electron microscopes has shown that steel 40, unlike steel 20, had a clearly defined so-called ‘white’ layer, as shown in Figs. 12 and 13. Obviously, with the content of a larger amount of carbon in the steel substrate, under specific cooling conditions during the ESA process, the surface layers undergo a noticeable martensitic transfor- mation. In this case, there is formed martensite with a greater degree of the crystal lattice tetragonality [91].

Due to the availability of the quenching processes, as well as a result of the increased carbon content in the surface layer, the microhardness of

Table 9. Distribution of chemical elements in the steel 40 surface layer after sulphocarburi- zing by the ESA method [86]

Surface point under investigation (step 10 to 20 μm)	Elements, %						
	S	Cu	Cr	Ni	Mn	Si	Fe
Steel 40, $W_p = 0.52$ J (step 20 μm)							
	0.68	—	—	—	0.58	2.95	102.22
	0.76	—	—	—	0.54	1.50	96.44
	0.08	—	—	—	0.58	1.16	94.70
	0.07	—	—	—	0.78	1.13	92.23
	0.33	—	—	—	0.58	1.01	98.44
	0.15	—	—	—	0.40	0.81	10.35
	0.13	—	—	—	0.48	8.21	36.13
	0.21	—	—	—	0.43	8.44	99.80
	0.03	—	—	—	0.52	6.24	24.11
	0.31	—	—	—	0.82	3.63	100.26
	0.21	—	—	—	0.66	0.83	104.59
Steel 40, $W_p = 0.13$ J (step 10 μm)							
	1.22	—	—	—	0.19	50.38	50.74
	0.54	—	—	—	0.29	40.87	19.07
	0.62	—	—	—	0.43	5.73	55.58
	0.72	—	—	—	0.49	5.09	73.79
	0.83	—	—	—	0.43	20.55	38.26
	0.40	—	—	—	0.32	37.74	25.57
	1.11	—	—	—	0.45	17.08	42.63
	1.35	—	—	—	0.35	3.64	83.39
	0.83	—	—	—	0.72	1.93	94.94
	0.25	—	—	—	0.76	1.83	96.20
	0.25	—	—	—	0.92	0.59	98.27

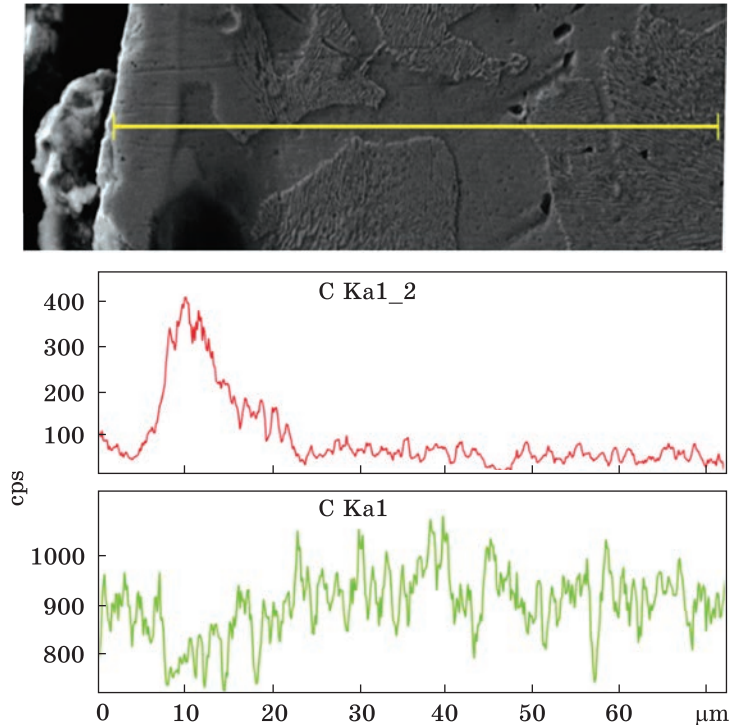


Fig. 14. Distribution of carbon and iron in the steel 40 surface layer after sulphocarburing by the ESA method at $W_p = 0.13$ J [86]

the layers obtained on steel 40 also becomes greater, as shown in Fig. 12: at $W_p = 0.13$ J, $H_\mu = 7074$ MPa, and at $W_p = 0.52$ J, $H_\mu = 13065$ MPa, as shown in Table 9. The continuity of the 'white' layer at $W_p = 0.13$ J is about 70%, and at $W_p = 0.52$ J, it tends to 100%.

The results of the micro-x-ray spectral analysis shown in Figs. 14–16 and Table 9 confirm our assumption relative the fact that during sulphocarburing by the ESA method, the surface layers at a depth of 10 to 40 μm , depending on the energy parameters of the process, have been being saturated with sulphur. This zone is a layer of reduced microhardness, and just as on steel 20, it is characterized by reduced microhardness shown in Fig. 12. Under this layer, a strengthened layer is formed. It is characterized by a high content of carbon as well as high microhardness. The thickness of the strengthened layer also depends on the energy parameters of the ESA process and is 15 to 40 μm .

Thus, the possibilities of using an energy-efficient and environmentally friendly process for simultaneously saturating with carbon and sulphur of the part steel surfaces by the ESA method have been studied. Because of the analysis of the surface layer topography after sulphocarburing by the ESA method, the uniform nature of the shape of the surface micro-roughness-formed elements has been established. A significant increase in the micro-roughness on the surface of the specimen is observed with an increase

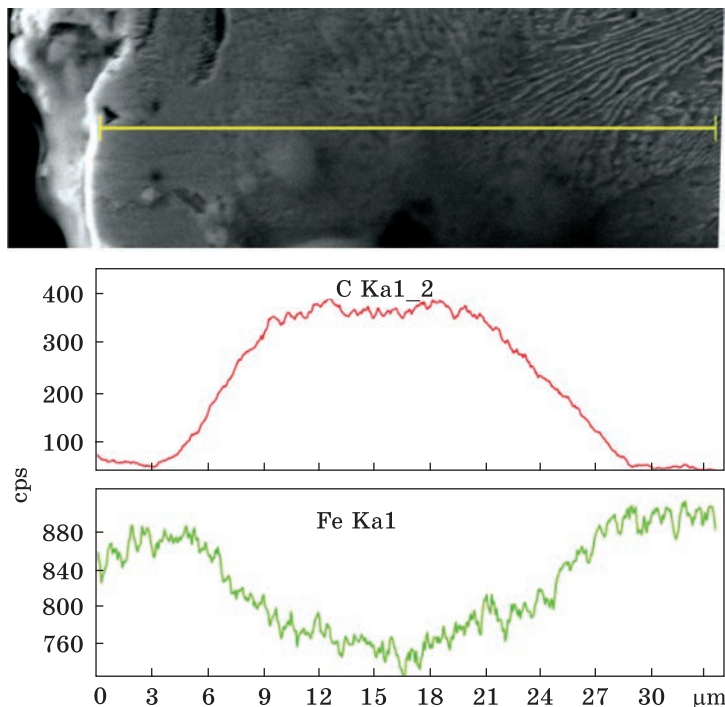


Fig. 15. Distribution of carbon and iron in the steel 40 surface layer after sulphocarburing by the ESA method at $W_p = 0.27$ J [86]

in the discharge energy up to $W_p = 3.4$ J. In this case, the surface roughness is $R_a = 2.5$ μm . The metallographic and durometric analyses after sulphocarburing by the ESA method have shown that the treated surface consists of such layers as a so-called soft layer, strengthened layer and base metal. At increasing the discharge energy, there is increase in the thickness, microhardness, and continuity of the coating. The presence of sulphur in a consistent substance contributes to the sulphurizing process.

With an increase in the discharge energy from 0.13 to 3.4 J for ESA processing steel 20, the amount of sulphur on the coating surface has been decreasing, however, due to intensifying the diffusion processes during passing an electric spark discharge, the thickness of the sulphurized layer has been increasing. Sulphur is accumulated in the surface of the metal at a depth of up to 30 μm . Its concentration at this distance is about 0.4%.

During sulphocarburing steel 40, the structure of the coating does not change. Due to the quenching processes, as well as because of the increased carbon content in the surface layer, the microhardness of the obtained layers on steel 40 increases: at $W_p = 0.13$ J, $H_\mu = 7074$ MPa, and at $W_p = 0.52$ J, $H_\mu = 13065$ MPa. The continuity of the white layer at $W_p = 0.13$ J is about 70%, and at $W_p = 0.52$ J, it tends to 100%.

The results of micro-x-ray spectral analysis of steel 40 specimens indicate that during sulphocarburing by the ESA method, the surface layers

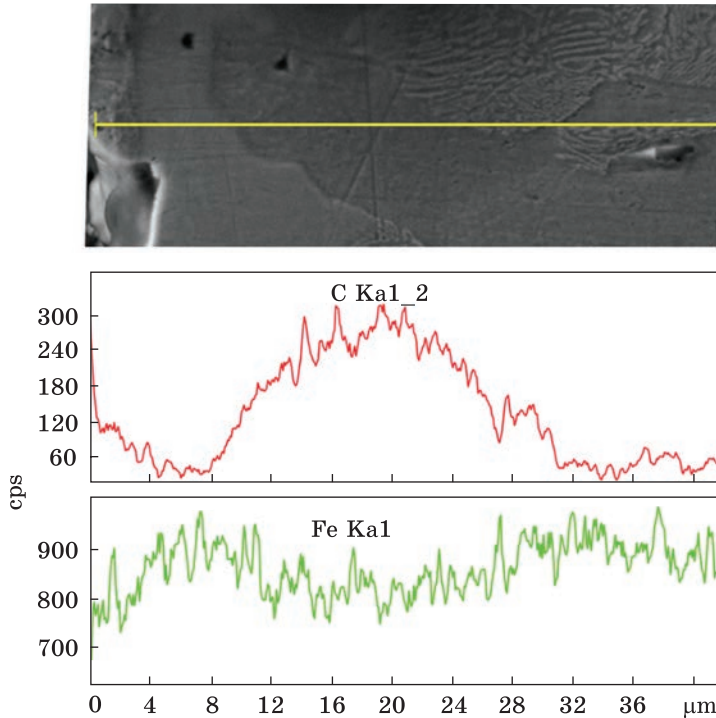


Fig. 16. Distribution of carbon and iron in the steel 40 surface layer after sulphocarburing by the ESA method at $W_p = 0.52$ J [86]

at a depth of 10 to 40 μm , depending on the energy parameters of the process, have been saturated with sulphur. This zone, namely, a layer of reduced microhardness, just as on steel 20, is characterized by the reduced microhardness. Under this layer, there is a strengthened layer, which is characterized by a high content of carbon and high microhardness. The thickness of the strengthened layer also depends on the energy parameters of the ESA process and comes to 15 to 40 μm .

3.3. Analysis of the Quality of the Sulphoaluminized Coatings Obtained by ESA Methods

The analysis of the specimen surface profiles after sulphoaluminizing by the ESA method and the roughness parameters of the surfaces calculated therefrom has shown that the parameters of R_a , R_z , R_{max} change depending on the discharge energy, as well as on the material of the base, as shown in Fig. 17. The parameters increase with an increase in discharge energy and carbon content in the base steel in Table 10.

Figures 18 and 19, respectively, show microstructures (a–c) and microhardness distribution (d) in the surface layer of steel 20 and steel 40 after sulphoaluminizing by the ESA method.

At replacing the material of the substrate with steel 40, there is increased hardness in both the upper layer (1670 and 2240 MPa at discharge

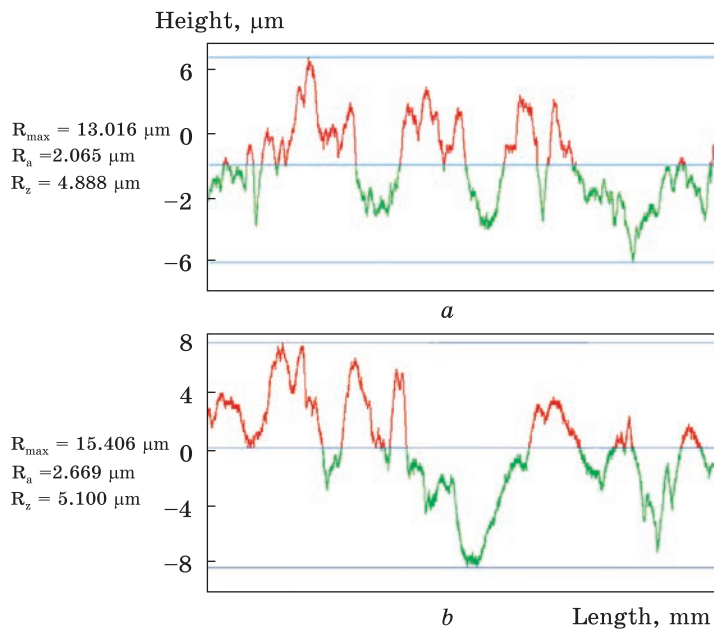


Fig. 17. Surface profilograms after sulphoaluminizing $W_p = 0.55 \text{ J}$: (a) steel 20; (b) steel 40 [90]

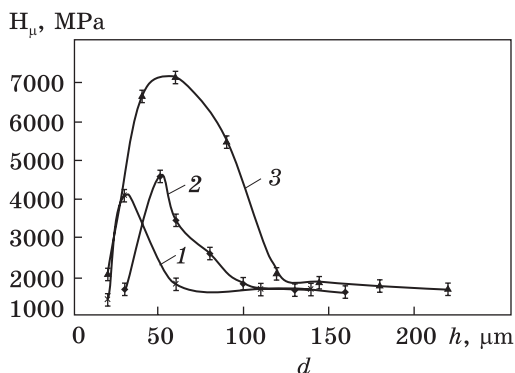
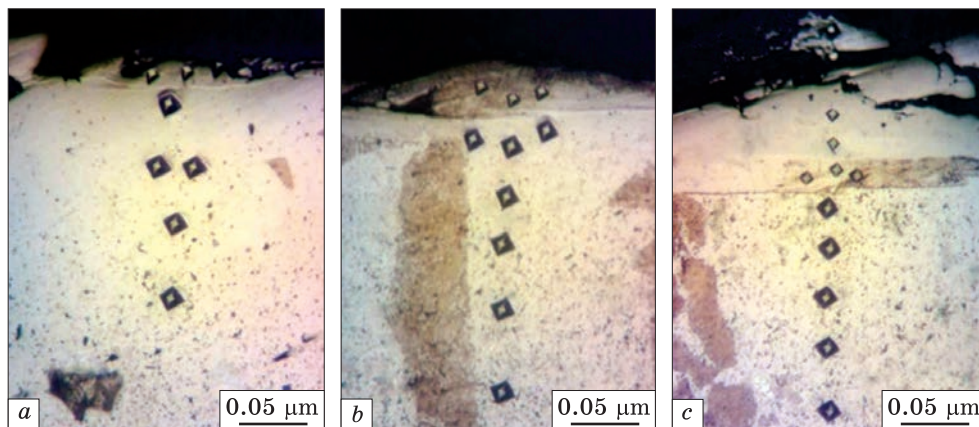


Fig. 18. Microstructures (a-c) and distribution of microhardness (d) in the surface layer of steel 20 after sulphoaluminizing by the ESA method: (a) $W_p = 0.13 \text{ J}$; (b) $W_p = 0.55 \text{ J}$; (c) $W_p = 3.4 \text{ J}$; (d) 1 — $W_p = 0.13 \text{ J}$, 2 — $W_p = 0.55 \text{ J}$, 3 — $W_p = 3.4 \text{ J}$ [89, 90]

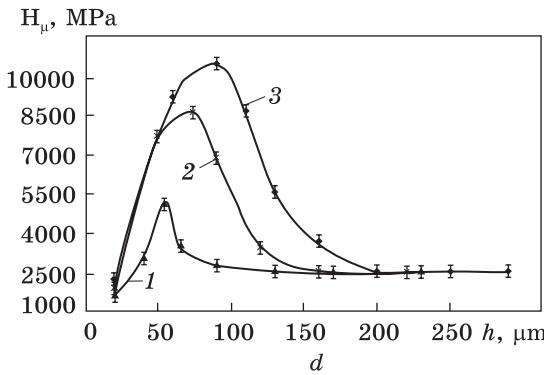
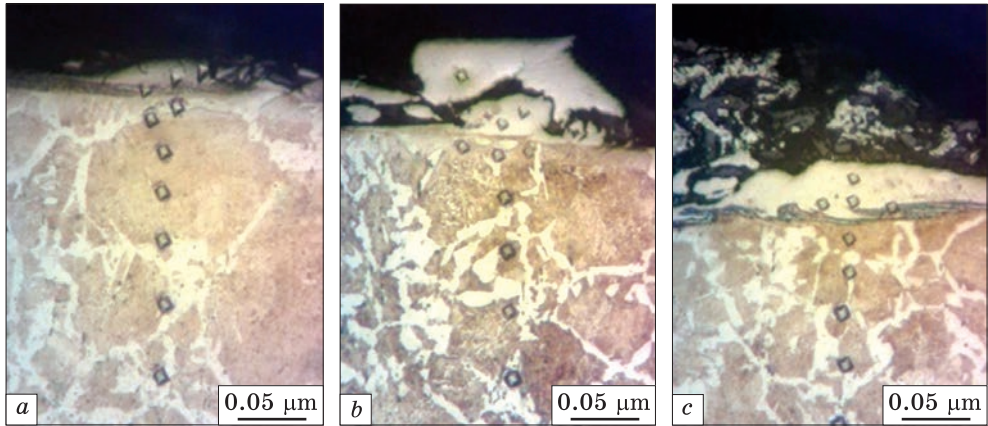


Fig. 19. Microstructures (a-c) and distribution of microhardness (d) in the surface layer of steel 40 after sulphoaluminizing by the ESA method: (a) $W_p = 0.13$ J; (b) $W_p = 0.55$ J; (c) $W_p = 3.4$ J; (d) 1 — $W_p = 0.13$ J, 2 — $W_p = 0.55$ J, 3 — $W_p = 3.4$ J [89, 90]

Table 10. Qualitative parameters of sulphoaluminized coatings obtained by the ESA method [89]

Discharge energy, J	Roughness, μm			Layer of reduced microhardness			Strengthened layer		
	R_a	R_z	R_{max}	H_μ , MPa	h , μm	S, %	H_μ , MPa	h , μm	S, %
Steel 20									
0.13	0.8	2.3	6.8	1368	40	50	4094	20	70
0.55	2.1	4.9	13.0	1666	30	65	4575	30	85
3.4	6.2	18.3	40.8	2073	20	80	7150	80	95
Steel 40									
0.13	0.9	2.6	7.1	1670	40	50	5147	20	75
0.55	2.7	5.1	15.4	1820	30	70	9123	40	90
3.4	6.1	18.7	38.8	2240	30	80	10380	70	95

energies of 0.13 and 3.4 J, respectively) and the strengthened layer (5147 and 10380 MPa at discharge energies of 0.13 and 3.4 J, respectively). An increase in microhardness with an increase in the carbon content of the substrate was also observed in other alloying processes, *i.e.*, in the aluminizing process [92–94] and in the sulphocarburing one [88]. Obviously,

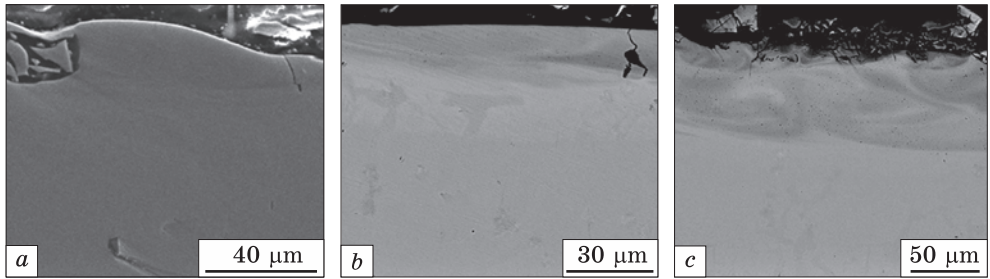


Fig. 20. The structures of the steel 40 surface layers after sulphoaluminizing by the ESA method: (a) $W_p = 0.13$ J; (b) $W_p = 0.55$ J; (c) $W_p = 3.4$ J [94]

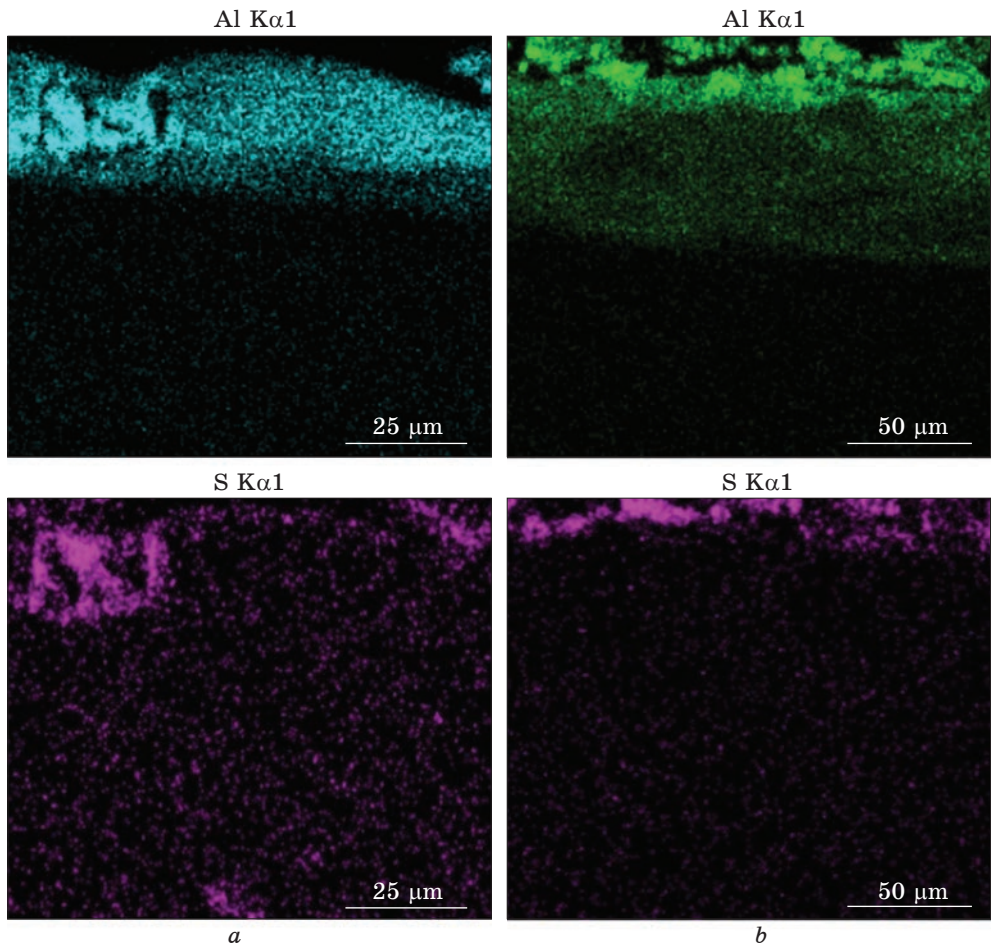


Fig. 21. Maps of chemical elements distribution in the coating after sulphoaluminizing steel 40 by the ESA method at different discharge energies: (a) $W_p = 0.13$ J; (b) $W_p = 3.4$ J [94]

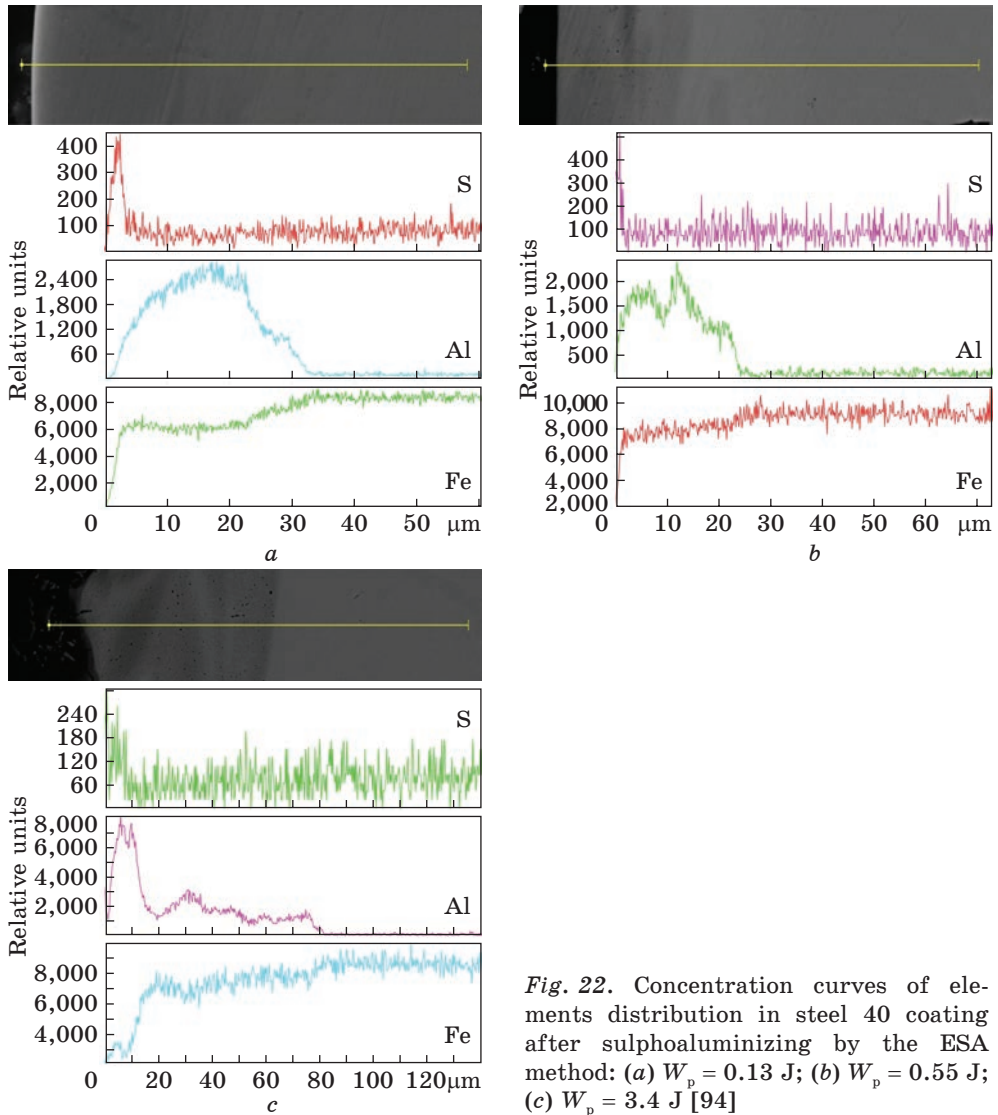


Fig. 22. Concentration curves of elements distribution in steel 40 coating after sulphoaluminizing by the ESA method: (a) $W_p = 0.13$ J; (b) $W_p = 0.55$ J; (c) $W_p = 3.4$ J [94]

the influence of the carbon content in the main material is caused by the formation of a multiphase quenching structure.

Electron-microscopy studies have indicated that due to the sulphoaluminizing process by the ESA method, high-quality layers of high continuity are formed, as shown in Fig. 20.

Figure 21 represents the maps of the distribution of sulphur and aluminium in the sulphoaluminized coatings obtained on different ESA modes. As research has shown, the largest amount of sulphur is accumulated in the surface layer and distributed at a depth of up to 10 μm . This

characterizes the layer as a layer of reduced microhardness. The diffusion zone of aluminium is of 30 to 80 μm , depending on the energy parameters of the ESA process. It should be noted that the highest aluminium content is characteristic of the areas of the coating located at a distance of 7 to 15 μm from the surface, as shown in Fig. 22. Therefore, the near-surface so-called soft layer is enriched with sulphur and strengthened with aluminium.

As evidenced by the results of x-ray studies, the phase composition of the coatings depends on the energy parameters of the ESA process, as well as on the carbon content in the base material. At all the investigated discharge energies, in the surface layer, there is formed intermetallic FeAl, and with increasing the discharge energy, this is FeAl₂ that is formed there, as shown in Figs. 23 and 24. In addition, a bcc solid solution is found in steel 20, and in steel 40 at the discharge energies of $W_p = 0.13$ J and $W_p = 0.55$ J, there is a f.c.c. solid solution, and at $W_p = 3.4$ J, there is a bcc solid solution in Tables 11 and 12.

The formation of the phase composition of sulphoaluminized coatings, the creation of sulphides and the change in their chemical composition significantly depend on the solubility and diffusion mobility of sulphur in

Table 11. Crystal lattice parameters and quantitative phase analysis of sulphoaluminized coatings on steel 20 [93]

Discharge energy, J	Phase	Lattice period a , nm	Phase content, mas. %	
0.13	FeAl	$a = 2.9040$	78.58	
	b.c.c. solid solution	$a = 2.8750$	21.42	
0.55	FeAl	$a = 2.9040$	79.25	
	b.c.c. solid solution	$a = 2.8750$	20.75	
3.4	FeAl	$a = 2.9040$	33.58	
	b.c.c. solid solution	$a = 2.8650$	10.58	
	FeAl ₂	$a = 4.8745$ $b = 6.4545$ $c = 8.7710$ $\alpha = 87.9300$ $\beta = 74.3960$ $\gamma = 83.0620$	47.49	
	Al	$a = 4.0610$	8.35	
	At a distance of 10 μm from the surface			
	FeAl	$a = 2.9040$	37.31	
	b.c.c. solid solution	$a = 2.8650$	10.52	
FeAl ₂	$a = 4.8745$ $b = 6.4545$ $c = 8.7710$ $\alpha = 87.9300$ $\beta = 74.3960$ $\gamma = 83.0620$	52.17		

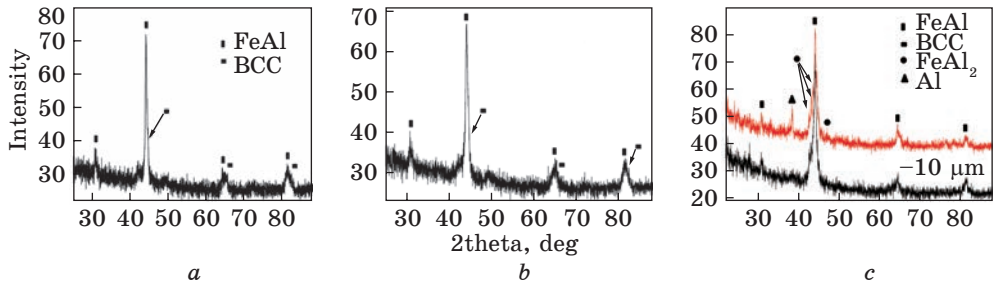


Fig. 23. Diffractograms of sulphoaluminized coatings obtained by the ESA method on steel 20: (a) $W_p = 0.13$ J; (b) $W_p = 0.55$ J; (c) $W_p = 3.4$ J [93, 95]

Table 12. Crystal lattice parameters and quantitative phase analysis of sulphoaluminized coatings on steel 40 [93]

Discharge energy, J	Phase	The period of the lattice a , nm	Phase content, mas. %
0.13	FeAl	$a = 2.8970$	85.37
	f.c.c. solid solution	$a = 3.6820$	14.63
0.55	FeAl	$a = 2.9040$	93.71
	f.c.c. solid solution	$a = 3.6980$	6.29
3.4	FeAl	$a = 2.9040$	36.72
	b.c.c. solid solution	$a = 2.8650$	13.60
	FeAl ₂	$a = 4.8745$	41.21
		$b = 6.4545$	
		$c = 8.7710$	
		$\alpha = 8.9300$	
		$\beta = 74.3960$	
		$\gamma = 83.0620$	
	Al	$a = 4.0610$	8.47
	At a distance of 10 μm from the surface		
FeAl	$a = 2.9040$	47.35	
b.c.c. solid solution	$a = 2.8800$	13.11	
FeAl ₂	$a = 4.8745$	39.55	
	$b = 6.4545$		
	$c = 8.7700$		
	$\alpha = 87.9300$		
	$\beta = 74.3960$		
	$\gamma = 83.0620$		

austenite and ferrite. In this regard, the diffusion of sulphur in iron and steel was studied in several works [95, 96]. It has been stated that the introduction of sulphur into alpha-iron reduces the carbon diffusion coefficient (D_0) and diffusion activation energy (Q) therein, as well as reduces the carbon solubility in it. Regarding the effect on the diffusion and solubility of carbon in α -iron, sulphur reveals itself as a typical non-carbide-

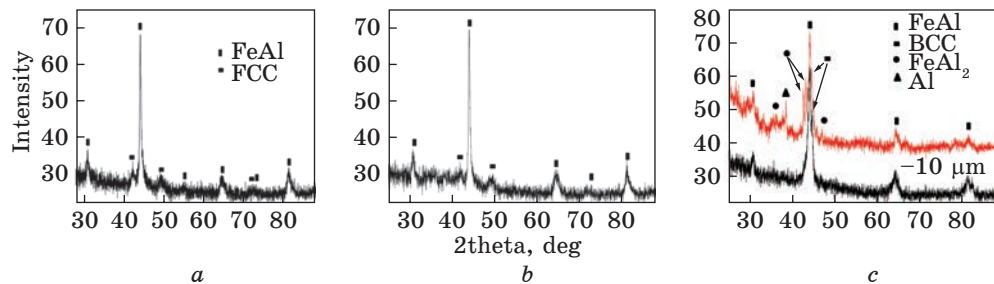


Fig. 24. Diffractograms of sulphoaluminized coatings obtained by the ESA method on steel 40: (a) $W_p = 0.13$ J; (b) $W_p = 0.55$ J; (c) $W_p = 3.4$ J [93, 95]

forming element. The influence of aluminium on the solubility of sulphur in gamma iron also has been investigated. The concentration curves of sulphur distribution obtained by the authors have shown that aluminium increases the solubility of sulphur in iron.

Obviously, due to the sulphur complex influence on the phase transformations in the surface layer of steel during the ESA process with the use of an aluminium electrode, sulphur dissolves in a solid solution and sulphides are not formed therein.

The availability of the peaks of the f.c.c. solid solutions on the diffractograms of the sulphoaluminized coatings on steel 40 at the discharge energies of $W_p = 0.13$ J and 0.55 J is a subsequence of the small thickness of the coatings (up to $40 \mu\text{m}$), the low coefficient of absorption of x-rays by aluminium, as well as of the higher degree of intensity for mixing the base material with the electrode material. In this regard, there is a possibility of fixing the phase composition of the transition zone located under the coating. Obviously, the formation of the f.c.c. solid solution is associated with alloying the base material, quenching medium-carbon steel during accelerated cooling, and, as a result, forming the residual austenite.

To create thick-layer coatings, the technology of sulphoaluminizing by the ESA method was tested according to the following scheme: mixing sulphur ointment and aluminium powder in the ratio of 33.3% S and 56% Al (by weight), ESA processing with an aluminium electrode at $W_p = 6.8$ J. Figure 25 shows the microstructure of the formed surface layer on a specimen of steel 20 and the distribution of the microhardness along the coating depth. A characteristic feature of the structure of the formed surface is a massive so-called white layer, the thickness of which is from 160 to $200 \mu\text{m}$ in some areas, as shown in Fig. 25, *a*. Microhardness on the surface is about 5000 MPa. From the surface to the base, the microhardness gradually has been decreasing, and at a depth of $170 \mu\text{m}$, it turns into microhardness of the base (1700 MPa).

The studies have shown that an increase in discharge energy does not lead to a significant strengthening of the surface layer. The microhard-

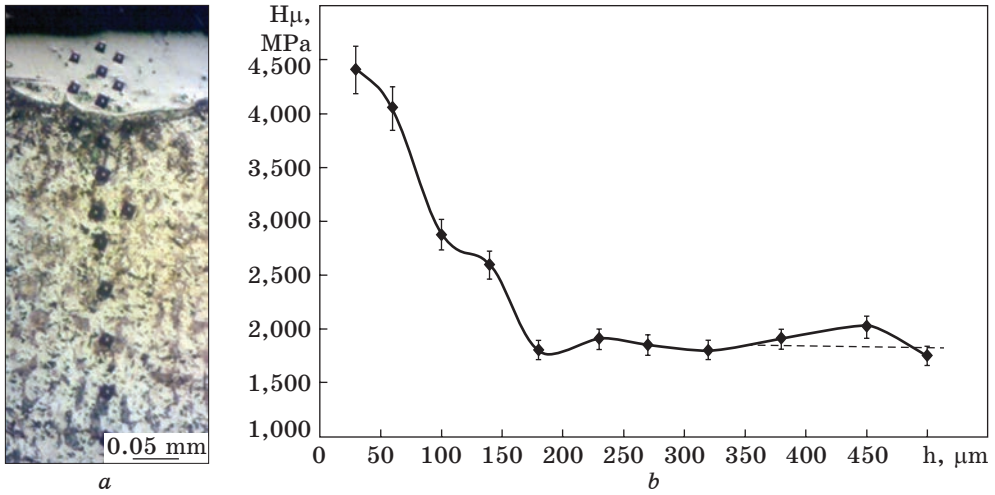


Fig. 25. Microstructure (a) and distribution of microhardness in the surface layer (b) of the specimen of steel 20 after the ESA process with aluminium electrode ($W_p = 6.8$ J) [92]

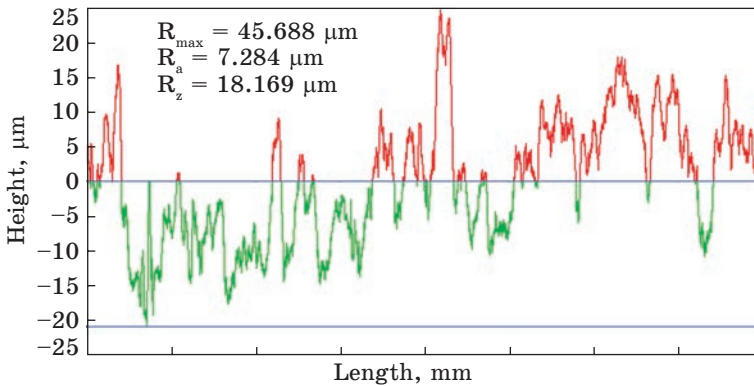


Fig. 26. Profilogram of a specimen surface made of steel 20 after sulphoaluminizing (33.3% S and 56% Al (wt.%) and the ESA process with the use of an aluminium electrode at $W_p = 6.8$ J) [89]

ness of the strengthened layer on steel 20 at $W_p = 3.4$ J is 7150 MPa, and at $W_p = 6.8$ J, it is about 5000 MPa, and in this case, the layer thickness increases from 80 up to 200 μm . However, with the increase in energy impact during the ESA process, there increases the surface roughness, as shown in Fig. 26. Thus, to obtain thick-layer sulphoaluminized coatings, there can be recommended the technology being considered.

Thus, the analysis of the surface profiles of the specimens after sulphoaluminizing process by the ESA method and the roughness parameters of the investigated surfaces have shown that with an increase in the discharge energy, as well as in the carbon content in steel, the R_a , R_z , R_{max}

parameters increase. Metallographic and durometric analyses of the obtained coatings on steel 20 indicate that the three zones can be distinguished on the microstructures, namely, a near-surface, non-continuous and loose layer of 10 to 100 μm thick and microhardness of 1368 to 2073 MPa, a so-called white strengthened layer of 20 to 40 μm thick and a microhardness of 4094 to 5157 MPa, a diffusion zone and a base metal having a ferrite-pearlite structure. It should be noted that while increasing W_p , there have been increasing the parameters of the layer, namely, thickness, microhardness of the upper and white layers, as well as their continuity. At replacing the material of the substrate with steel 40, the hardness of the upper layer increases (1670 and 2240 MPa at $W_p = 0.13$ and 3.4 J, respectively) and of the strengthened layer (5147 and 10380 MPa at $W_p = 0.13$ and 3, 4 J respectively). Local micro-x-ray spectral analysis has shown that the largest amount of sulphur is in the surface layer, which is distributed to a depth of up to 10 μm , characterizes the layer as the one of reduced microhardness. The diffusion zone of aluminium is of 30 to 80 μm , depending on the energy parameters of the ESA process. The highest aluminium content is characteristic of the areas of the coating located at a distance of 7 to 15 μm from the surface. The near-surface so-called soft layer is enriched with sulphur, and it is strengthened with aluminium.

As evidenced by the results of x-ray studies, the phase composition of the coatings depends on the energy parameters of the ESA process, as well as on carbon content in the base material. At all the investigated W_p , the intermetallic FeAl is formed. With an increase in W_p , there an intermetallic FeAl₂ is formed. In addition, a bcc solid solution is found in steel 20. In steel 40, at $W_p = 0.13$ J and at $W_p = 0.55$ J, an f.c.c. solid solution is created, and at $W_p = 3.4$ J, there is a bcc solid solution.

3.4. Analysis of the Quality of Al–C–S Coatings Obtained via the ESA Methods

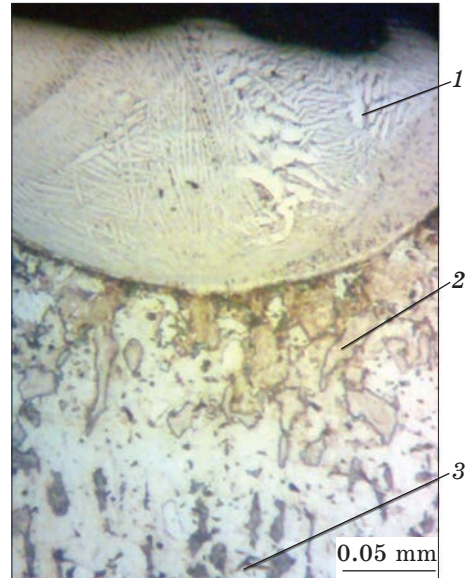
The complex Al–C–S coatings have been obtained by the ESA method according to the technology represented in Table 13.

The microstructural analysis of the specimens has shown that in the surface layer, the formation of individual indentations having a depth of up to 150 μm is observed. As shown in [91], at passing an electric spark discharge through a metal, therein, an indentation is formed, namely, a crater, the depth and diameter of which depend on the parameters of the

Table 13. Technology for obtaining complex Al–C–S coatings [96]

Consistent substance composition	Alloying electrode (anode)
33.3% S + 56% Al (wt.%)	graphite

Fig. 27. Microstructure of a steel 20 specimen: 1, 2, 3 — zones in the crater area (the electrode is graphite, $W_p = 6.8$ J, before the ESA process, the surface of the steel 20 specimen has been covered with a consistent substance containing 33.3% of sulphur and 56% of aluminium powder) [96]



electric spark effect. The spark discharge is accompanied by the release of heat. The temperature rise rate is $105\text{ }^\circ\text{C/s}$, which is characteristic only for explosive processes [97–99]. According to the work of [100], about 25% of the volume of the metal of the electrical erosion craters reaches the boiling point. The instantaneous pressures on the surfaces reach hundreds of thousands of atmospheres.

On the specimens of steel 20, there are distinguished three zones in the area of the crater, as shown in Fig. 27.

The first zone is a melting one. It is poorly etched; the metal in this zone is in a liquid state in the course of the ESA process. This zone consists of columnar crystals; the high rate of crystallization determines the anisotropy of crystal growth, that is, the accelerated growth of the main axes of dendrites oriented in the direction of heat removal. The thickness of the layer of the columnar crystals on the side surface increases from the

Table 14. Qualitative parameters of the surface layers of the Al-C-S system, which have been obtained by the ESA method on steel 20 and steel 40 [96]

Discharge energy, J	White layer thickness, μm	White layer microhardness, MPa	Roughness, μm			White layer continuity, %
			R_a	R_z	R_{max}	
Steel 20						
0.52	150	9300 ± 50	2.1	3.9	8.9	90
2.60	110	9200 ± 70	4.2	8.7	30.2	80
6.8	up to 60	9000 ± 50	8.5	1.2	62.4	50
In stages 6.8 and 2.6	up to 60	9000 ± 50	4.3	8.4	32.3	70
In stages 6.8; 2.6 and 0.52	up to 60	9000 ± 50	2.6	4.4	11.5	80
Steel 40						
0.52	up to 180	9500 ± 50	1.9	3.8	8.7	90
2.60	up to 130	9300 ± 50	3.9	8.5	15.3	80
6.8	up to 80	9100 ± 50	7.8	11.3	58.1	60

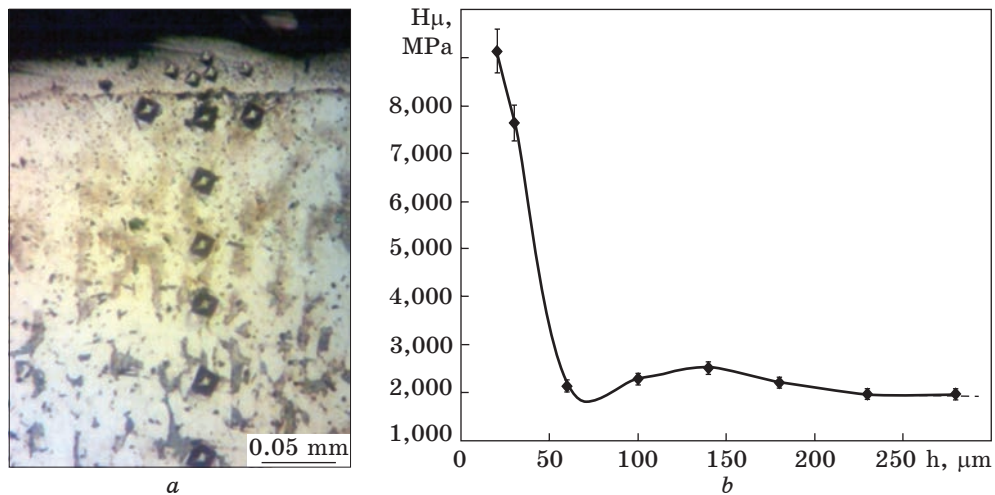


Fig. 28. Microstructure (a) and distribution of microhardness in the surface layer (b) of steel 20 specimen after the ESA process with graphite ($W_p = 6.8$ J) [90]

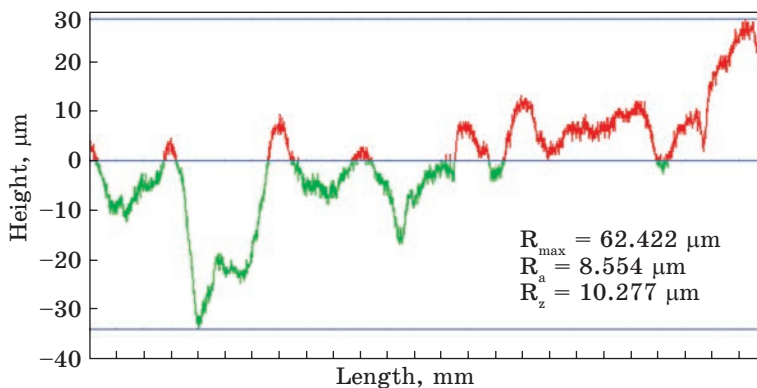


Fig. 29. The profilograms of the steel 20 specimen surface layers (33.3% S + 56% Al (wt.%)), ESA process with a graphite electrode at $W_p = 6.8$ J) [97]

The second zone is a transition zone, which is adjacent to the first one and consists of grains of a complex shape. This is a zone of thermal influence.

The third zone is a zone of the original metal. It is adjacent to the first two and has an original structure.

There has been studied the effect of the ESA modes on the quality parameters of the Al-C-S coatings.

The microstructural analysis of the Al-C-S coatings on steel 20 has shown (Fig. 28, a) that the co-called white layer is formed on the surface. It is followed by the diffusion zone and the base metal. Also it should be noted that at ESA processing the steel 20 with graphite, the continuity and thickness of the white layer is 50% and 60 μm , respectively (at $W_p =$

= 6.8 J). In turn, the microhardness on the surface is 9000 MPa, shown in Fig. 28, *b* and Table 14. In Ref. [88], it was shown that in the course of electrospark processing the iron-based alloys, there is a significant decrease in the size of the substructure blocks, an increase in the density of defects, and an increase in micro distortions in the thermally affected zone. Such changes in the microstructure and substructure of the steel lead to a noticeable increase in the microhardness of the white layer in Fig. 28. Such elements of the atmosphere as nitrogen and oxygen can play a certain role in increasing hardness. Passing under the action of electric discharges into an active state, they can interact with the surface layers and strengthen the material.

The availability of sulphur in the consistent substance contributes to the sulphurizing process. Table 15 shows the change in the sulphur content by depth from the surface of steel 20 after the ESA process at discharge energy of 6.80 J. Thus, the amount of sulphur is maximal on the surface and it has been decreasing while it is moving away from the surface.

It should be noted that, at simultaneously saturating steel with carbon, sulphur and aluminium by the ESA method, with a significant increase in the discharge energy (from 0.52 to 6.8 J), there is an increase in the surface roughness and a decrease in the continuity of the coating in Table 15. Figure 34 shows the surface profilogram of the sample after the ESA process.

The investigation of simultaneously saturating the 38X2MIOA (38Kh2MUA) steel with carbon, sulphur and aluminium by the ESA method using a graphite electrode at different modes has been carried out. The metallographic analysis has shown that the coatings obtained at $W_p = 0.13$ J

Table 15. Sulphur content in the surface layer of steel 20 at simultaneously saturating steel with carbon, sulphur and aluminium by the ESA method [97]

Distance from the surface, μm	20	40	60	80	100	120	140	160	180
Sulphur content, %	0.21	0.15	0.12	0.09	0.08	0.05	0.05	0.03	0.03

Table 16. Qualitative parameters of surface layers during simultaneously saturating of 38X2MIOA (38Kh2MUA) steel with carbon, sulphur and aluminium by the ESA method [98]

Discharge energy, J	White layer thickness, μm	White layer micro-hardness, MPa	Roughness, μm			White layer continuity, %
			R_a	R_z	R_{max}	
0.13	10	5126	0.8	2.1	6.5	60
0.52	30	5890	2.3	4.4	15.1	90
4.9	70	7721	8.2	18.3	47.3	100

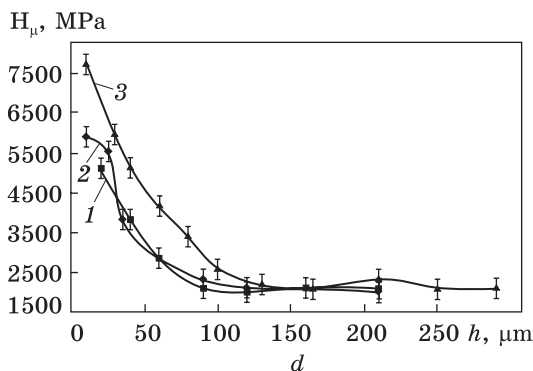
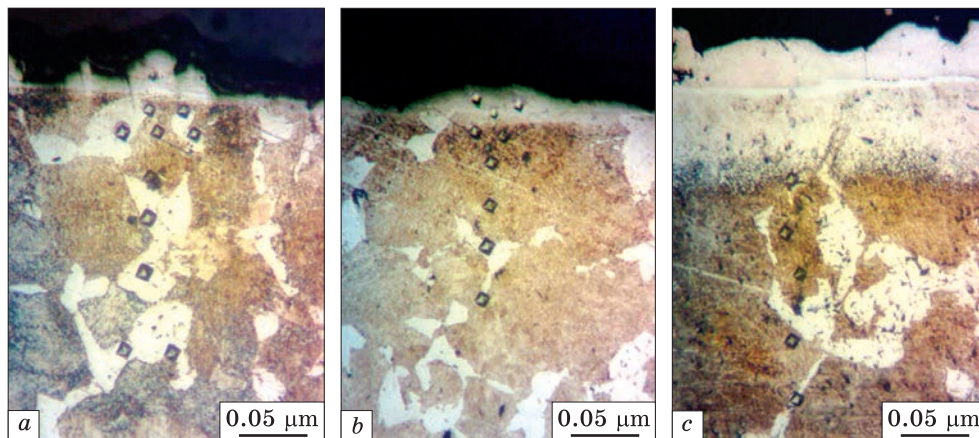


Fig. 30. Microstructures (a-c) and distribution of microhardness in the surface layer (d) of 38X2MIOA (38Kh2MUA) steel specimens after saturating with sulphur, aluminium, and carbon by the ESA method: (a) $W_p = 0.13$ J; (b) $W_p = 0.52$ J; (c) $W_p = 4.9$ J; (d) 1 — $W_p = 0.13$ J, 2 — $W_p = 0.52$ J, 3 — $W_p = 4.9$ J [96]

and $W_p = 0.52$ J consist of 3 zones, as shown in Fig. 29: 1) white layer, 2) transition zone, and 3) base metal.

However, with an increase in the discharge energy up to 4.9 J, a sub-layer of up to 10 μm thick is formed between the white layer and the transition zone, as shown in Fig. 30, c. In addition, as the discharge energy increases, the thickness of the white layer and its continuity also increase in Table 16. Therefore, at $W_p = 0.13$ J and $W_p = 4.9$ J, the thickness of the white layer is 10 and 70 μm , and the continuity is 60 and 100%, respectively.

Durometric studies have shown that the microhardness of the white layer increases as the discharge energy increases. Thus, at the discharge energy of $W_p = 0.13$ J, $H_\mu = 5126$ MPa, and the discharge energy of $W_p = 4.9$ J, $H_\mu = 7721$ MPa, as shown in Fig. 30.

The discharge energy, at which the ESA process takes place, affects the distribution of elements in the resulting coating. The analysis of Fig. 31 has shown that with an increase in the discharge energy, on the surface of the coatings, a decrease for sulphur is observed. Probably, it is related to burning of sulphur when a pulsed discharge occurs in the ESA process.

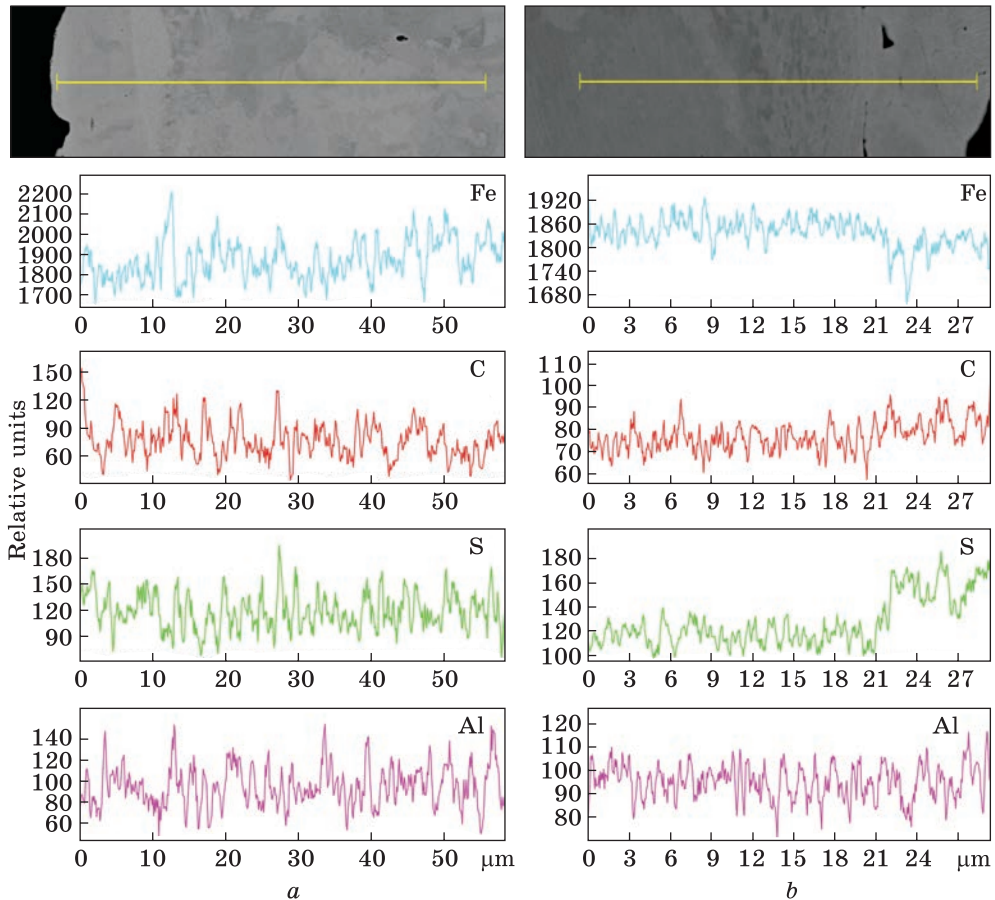


Fig. 31. Distribution of elements in the Al-C-S coating obtained by the ESA method: (a) $W_p = 0.13$ J; (b) $W_p = 4.9$ J [98]

Thus, the features of structure formation of Al-C-S coatings obtained by the ESA method have been investigated. It has been shown that the formation of the individual indentations of up to 150 μm in depth has been observed in the surface layer. On the steel 20 specimen, the three zones can be distinguished in the area of the crater. Those are as follows: the first zone is a melting one. It is poorly etched. The metal of this zone is in a liquid state during the ESA process. The second one is a transition zone. It is adjacent to the first zone and consists of grains of a complex shape. This is a zone of thermal influence. The third the zone is of the original metal. It is adjacent to the first two zones and has an original structure. There has been studied the effect of the ESA modes on the quality parameters of the Al-C-S system coatings. With a significant increase in the discharge energy (from 0.52 to 6.8 J), there is an increase in the surface roughness and a decrease in the continuity of the coating.

Table 17. Qualitative parameters of sulphomolibdenized coatings obtained by the ESA method [102]

Discharge energy, J	Roughness, μm			Reduced microhardness layer			Strengthened layer		
	R_a	R_z	R_{max}	H_μ , MPa	h , μm	S, %	H_μ , MPa	h , μm	S, %
Steel 20									
0.13	0.6	2.1	6.1	1112	20	45	5147	20	65
0.55	1.9	3.3	14.2	1368	30	65	7150	30	75
3.4	5.5	14.7	38.5	1666	40	75	10596	50	90
Steel 40									
0.13	0.8	2.3	6.5	1320	10	50	5474	25	75
0.55	2.0	3.5	14.7	1670	20	70	7832	40	90
3.4	5.7	14.9	38.7	2040	30	80	10731	70	95

The microstructural analysis of the Al-C-S coatings on steel 20 has shown that the continuity and thickness of the white layer are 50% and 60 μm , respectively (at $W_p = 6.8$ J). In turn, the microhardness on the surface is 9000 MPa. The availability of sulphur in the consistent substance contributes to the sulphurizing process. The amount of sulphur is maximal on the surface and has been decreasing with distance from the surface. There was carried out investigation of the process for simultaneously saturating the 38X2MIOA (38Kh2MUA) steel with carbon, sulphur and aluminium by the ESA method with a graphite electrode on different modes. The metallographic analysis has shown that the coatings obtained at $W_p = 0.13$ J and 0.52 J consist of the following 3 zones: a white layer, a transition zone and the base metal. However, with an increase in discharge energy up to 4.9 J, a sublayer with a thickness of up to 10 μm has been formed between the white layer and the transition zone. In addition, with an increase in the discharge energy, the thickness of the white layer, its microhardness and continuity have been increasing. Thus, at $W_p = 0.13$ J and $W_p = 4.9$ J, the thickness of the white layer is 10 and 70 μm , $H_\mu = 5126$ MPa and $H_\mu = 7721$ MPa, the continuity is 60 and 100%, respectively. The x-ray microspectral analysis has showed that the sulphur content is maximal on the surface and sharply decreases in the depth of the metal.

3.5. Analysis of the Quality of Sulphomolibdenized Coatings Obtained by the ESA Methods

In work [102], a method for sulphomolibdenizing metal surfaces is proposed. It consists in applying the special technical substance (STS) containing sulphur and electrospark alloying (ESA) by a molybdenum electrode at discharge energies of 0.13, 0.55, 3.4 J in Table 17.

Metallographic and durometric studies have shown that sulphomolibdenized coatings consist of the following 4 zones: the upper loose layer with

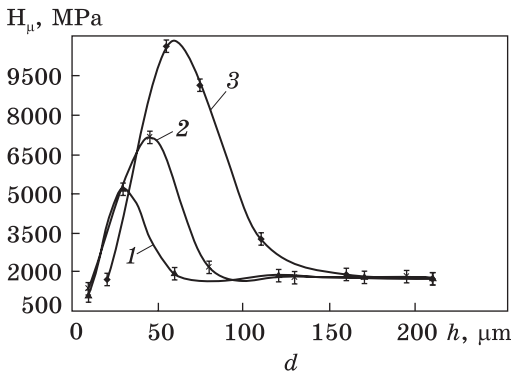
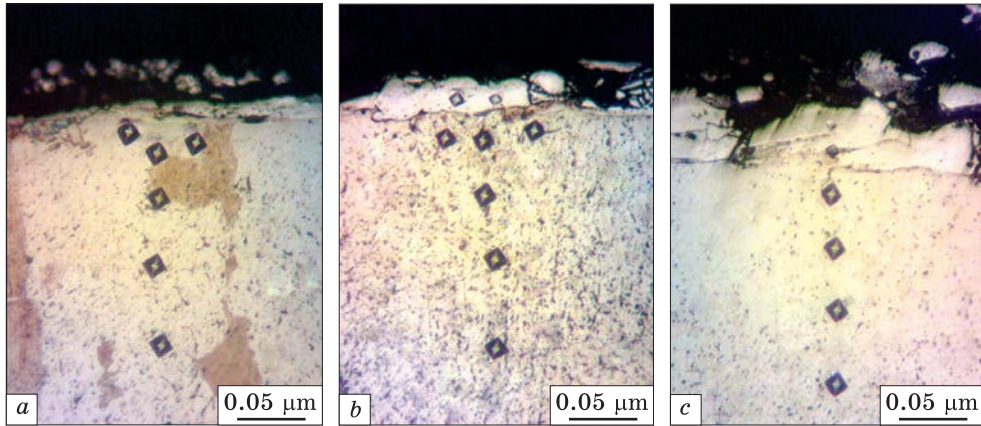


Fig. 32. Microstructures (a-c) and distribution of microhardness (d) in the surface layer of steel 20 after sulphomolibdenizing by the ESA method [100]: (a) $W_p = 0.13$ J; (b) $W_p = 0.55$ J; (c) $W_p = 3.4$ J; (d) 1 — $W_p = 0.13$ J, 2 — $W_p = 0.55$ J, 3 — $W_p = 3.4$ J [102]

Table 18. Crystal lattice parameters and quantitative phase analysis of sulphomolibdenized coatings on steel 40 [102]

Discharge energy, J	Phase	Lattice period a , nm	Phase content, mas. %
0.55	b.c.c. solid solution	2.8720	23.90
	f.c.c. solid solution	3.6450	25.38
	Martensite	$a = 2.8740$ $c = 2.9200$	10.98
	FeMo (σ -phase)	$a = 9.1280$ $c = 4.8130$	39.74
3.4	At a distance of 15 μm		
	b.c.c. solid solution	2.8720	46.36
	f.c.c. solid solution	3.6450	6.10
	Martensite	$a = 2.8640$ $c = 2.9200$	30.14
	FeMo (σ -phase)	$a = 9.1280$ $c = 4.8130$	12.53
	MoS ₂	$a = 3.1212$ $c = 12.2410$	4.87

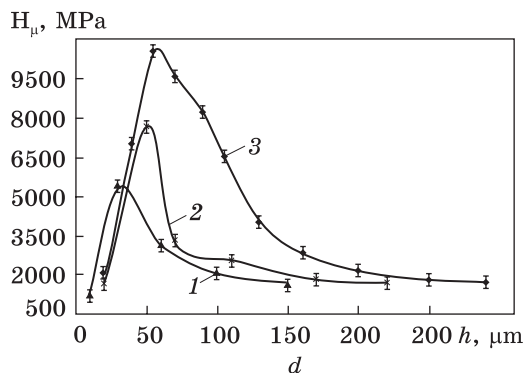
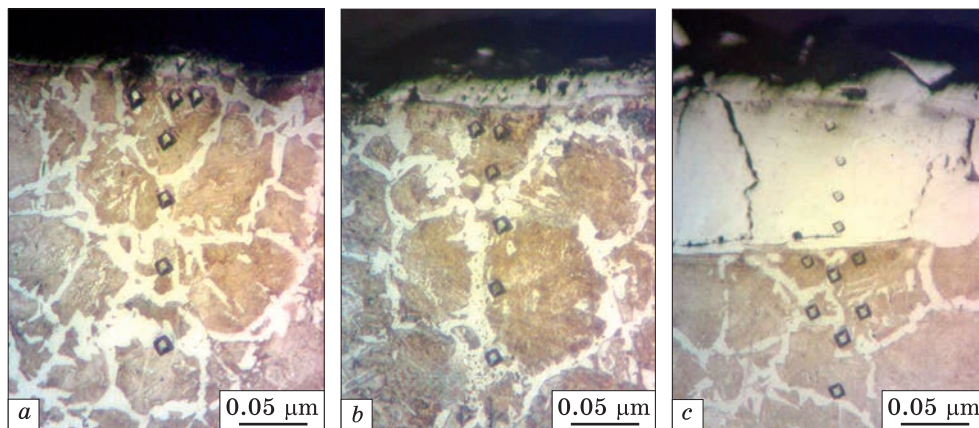


Fig. 33. Microstructures (a-c) and distribution of microhardness (d) in the surface layer of steel 40 after sulphomolibdenizing by the ESA method (a) $W_p = 0.13 \text{ J}$; (b) $W_p = 0.55 \text{ J}$; (c) $W_p = 3.4 \text{ J}$; (d) 1 — $W_p = 0.13 \text{ J}$, 2 — $W_p = 0.55 \text{ J}$, 3 — $W_p = 3.4 \text{ J}$ [102]

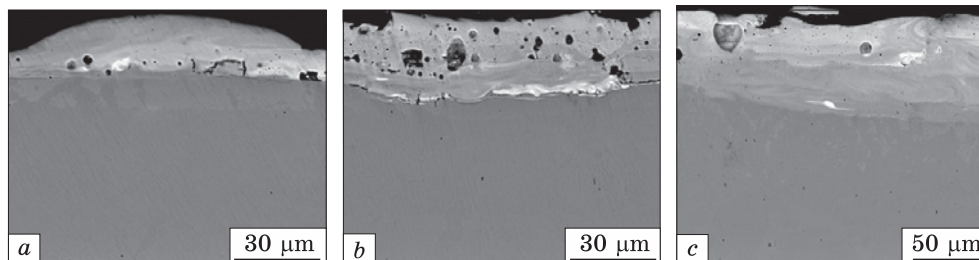


Fig. 34. Results of electron microscopic studies of sulphomolibdenized coatings on steel 40 obtained by the ESA method: (a) $W_p = 0.13 \text{ J}$; (b) $W_p = 0.55 \text{ J}$; (c) $W_p = 3.4 \text{ J}$ [103]

the microhardness of $H_\mu = 1112\text{--}2040 \text{ MPa}$, the white strengthened layer with $H_\mu = 5147\text{--}5474 \text{ MPa}$ for $W_p = 0.13 \text{ J}$ and $H_\mu = 10596\text{--}10731 \text{ MPa}$ for $W_p = 3.4 \text{ J}$, the diffusion zone and the base metal, as shown in Figs. 32 and 33. When replacing the substrate made of steel 20 by the one made of steel 40, there is an increase in microhardness, thickness of the strengthened layer, as well as in continuity seen in Table 17.

The analysis of the surface area containing the coating and a fragment of the base metal having a pre-eutectoid structure has shown that the ob-

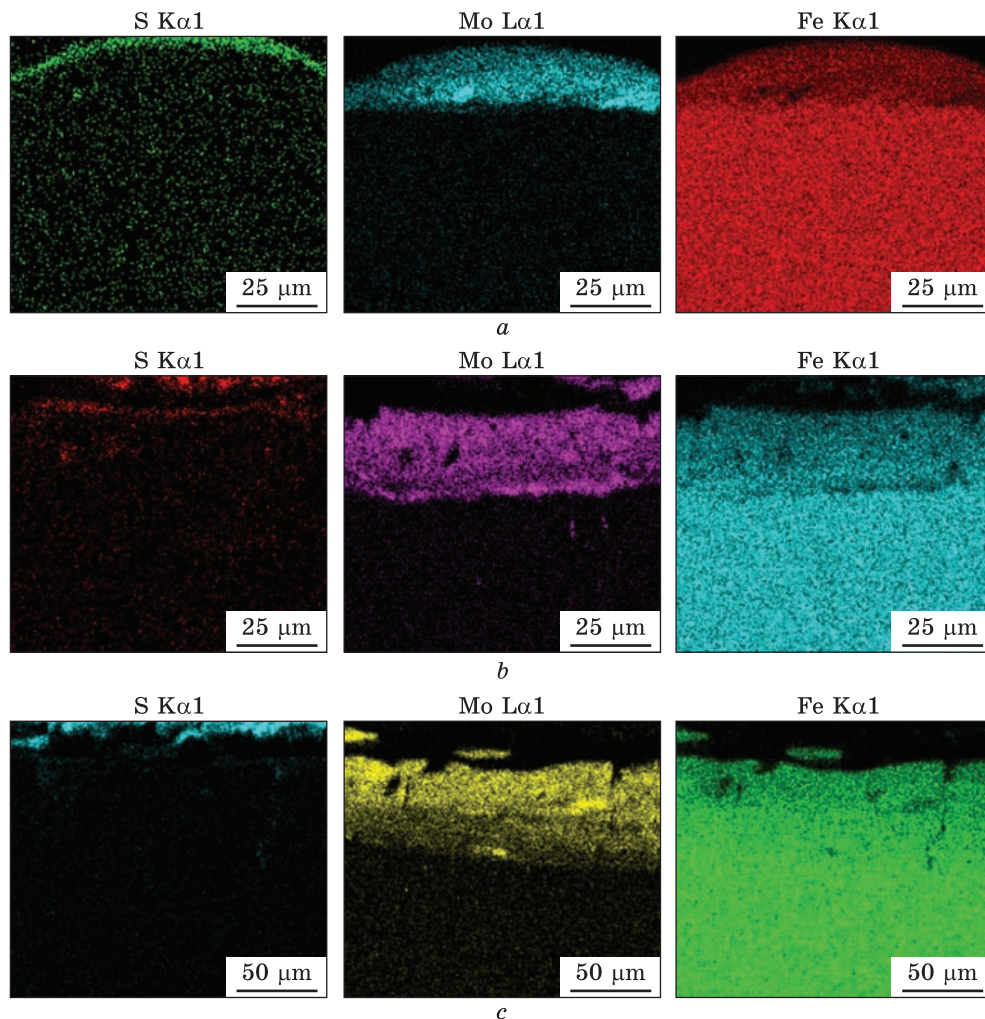


Fig. 35. Maps of the distribution of chemical elements in the coating after sulphomolibdenizing steel 40 by the ESA method at different discharge energies: (a) $W_p = 0.13$ J; (b) $W_p = 0.55$ J; (c) $W_p = 3.4$ J [103]

tained layer has a heterogeneous composition with different concentrations of elements, as shown in Fig. 34. Thus, according to the maps of the distribution of the elements over the areas of the specimens being studied, as seen in Fig. 35, sulphur is concentrated on the surface, and molybdenum is distributed more evenly in the coating.

According to the result of the local energy dispersive x-ray microanalysis, the distribution curves for sulphur, molybdenum, and iron have been obtained, as shown in Fig. 36. It is shown that sulphur and molybdenum are concentrated at a depth of up to 4 and 19 μm , respectively,

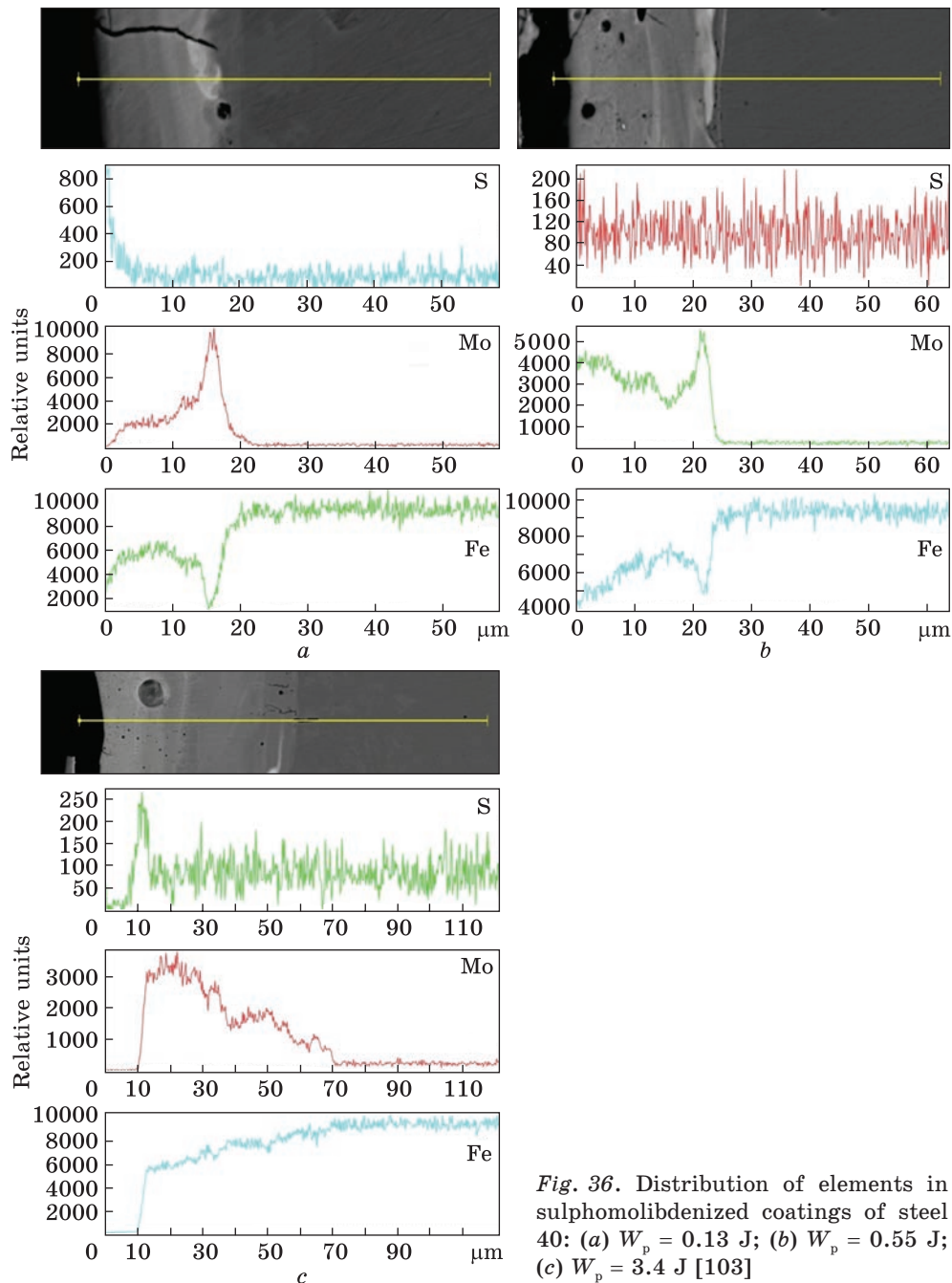


Fig. 36. Distribution of elements in sulphomolibdenized coatings of steel 40: (a) $W_p = 0.13$ J; (b) $W_p = 0.55$ J; (c) $W_p = 3.4$ J [103]

at $W_p = 0.13$ J, at 5 and 25 μm at $W_p = 0.55$ J; and at 15 and 70 μm at $W_p = 3.4$ J, respectively. The x-ray structural analysis of the obtained coatings confirms the results of the energy dispersion analysis seen in

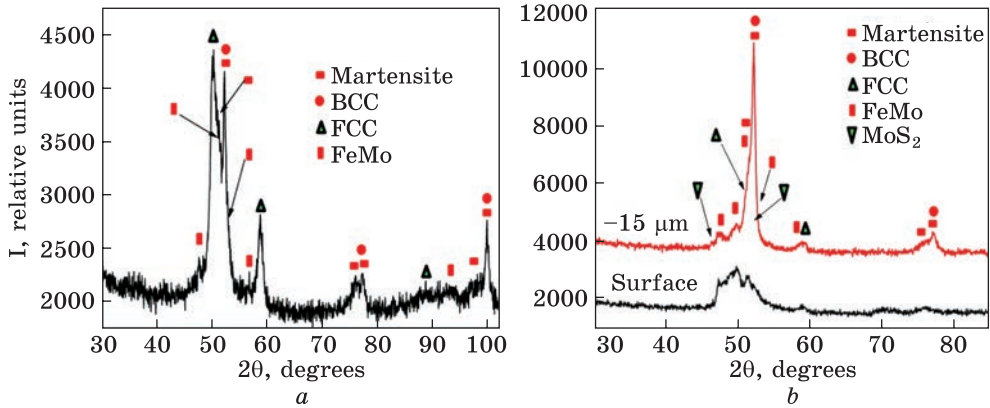


Fig. 37. Diffraction patterns of sulphomolibdenized coatings obtained by the ESA method on steel 40: (a) $W_p = 0.55$ J; (b) $W_p = 3.4$ J [102, 104]

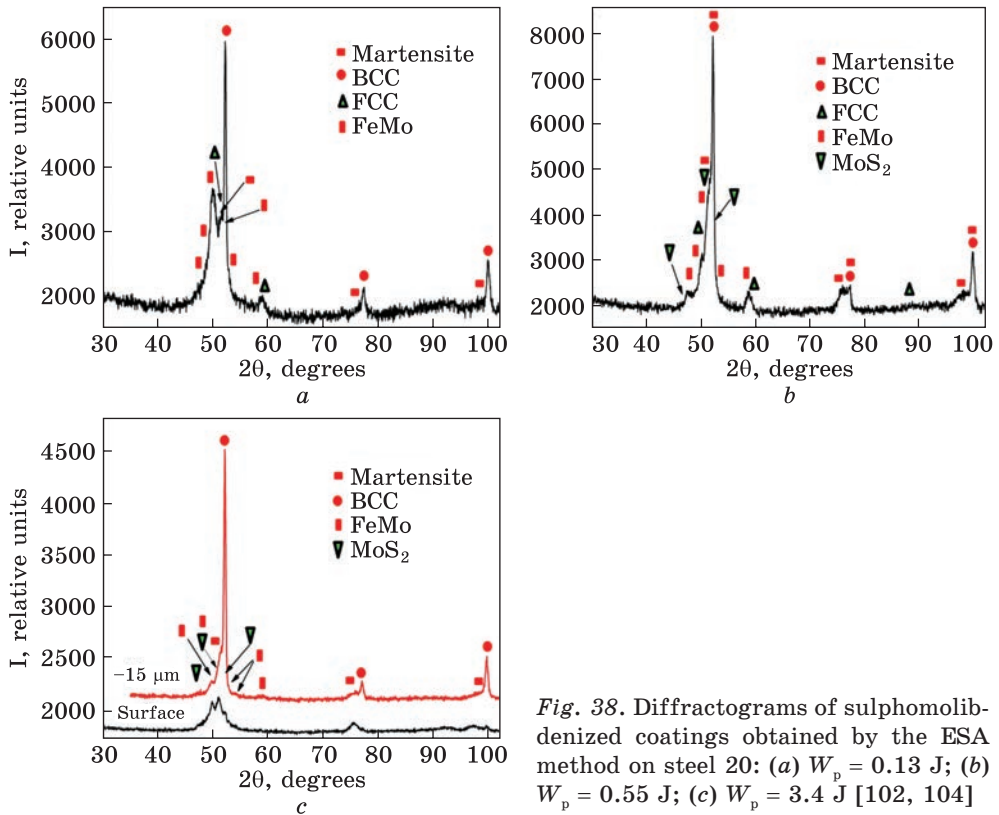


Fig. 38. Diffraction patterns of sulphomolibdenized coatings obtained by the ESA method on steel 20: (a) $W_p = 0.13$ J; (b) $W_p = 0.55$ J; (c) $W_p = 3.4$ J [102, 104]

Fig. 37. Thus, at low discharge energies, the phase composition of the coatings on steel 40 is represented by a bcc solid solution with a lattice period close to ferrite, martensite, an f.c.c. solid solution, and FeMo in-

termetallic (σ -phase). Obviously, in connection with alloying the bcc solid solution (ferrite) with sulphur and molybdenum, non-equilibrium cooling conditions, there is an increased lattice period, as shown in Table 18.

Under the conditions of high rates of heating and cooling of the microvolumes of the surface layers, which lead to the formation of non-equilibrium structures, as well as, due to mixing the base material with the material of the alloying electrode, the interaction of the liquid bath of the alloy in the course of the ESA process with the environment such as an atmospheric air, and also because of the intense shock waves, which arise during the ESA and result in the thermomechanical strengthening and other events affecting the phase formation, obviously, two alloyed austenites have been forming in the surface layer at the alloying temperature (more than 1000 °C). One of them, the Mn martensitic point of which is at above room temperature, undergoes a martensitic transformation upon cooling. In this case, the martensite with the lattice parameters $a = 2.8740$ nm and $c = 2.9200$ nm is formed. Because molybdenum intensively lowers the temperatures of the martensitic transformations, these proces-

Table 19. Crystal lattice parameters and quantitative phase analysis of sulphomolibdenized coatings on steel 20 [102]

Discharge energy, J	Phase	Lattice period a , nm	Phase content, mas. %
0.13	b.c.c. solid solution	2.8720	39.43
	Martensite	$a = 2.8640$ $c = 2.9200$	18.92
	FeMo (σ -phase)	$a = 9.1280$ $c = 4.8130$	25.50
	f.c.c. solid solution	$a = 3.6450$	16.15
0.55	b.c.c. solid solution	2.8720	34.92
	f.c.c. solid solution	3.6450	13.72
	Martensite	$a = 2.8640$ $c = 2.9200$	30.46
	FeMo (σ -phase)	$a = 9.1280$ $c = 4.8130$	17.14
	MoS ₂	$a = 3.1212$ $c = 12.2400$	3.77
3.4	At a distance of 15 μ m		
	b.c.c. solid solution	2.8800	59.86
	Martensite	$a = 2.8640$ $c = 2.9200$	25.46
	FeMo (σ -phase)	$a = 9.1280$ $c = 4.8130$	9.56
	MoS ₂	$a = 3.1212$ $c = 12.2400$	5.12

ses do not occur until the end, that is, until they are completed. Therefore, some amount of the residual austenite, namely, a solid solution of f.c.c., remains untransformed in the coating, as shown in Table 18. In addition to the solid solutions, in the surface layer, there are formed up to 40% of FeMo intermetallics, which contributes to a noticeable increase in the microhardness of the surface layer after the ESA process at $W_p = 0.55$ J (at $W_p = 0.13$ J, $H_\mu = 5474$ MPa; at $W_p = 0.55$ J, $H_\mu = 7832$ MPa, Table 17.

Sulphomolibdenizing steel 40 by the ESA method at $W_p = 3.4$ J leads to an increase in the amount of the martensitic phase up to 30%, as compared to 11% at $W_p = 0.55$ J, decrease for austenite (f.c.c. phase) from 25% to 6%, as well as to 5% of molybdenum disulphide. It should be noted that with increasing the discharge energy, there has been increasing the surface roughness, which makes it impossible to obtain reliable results from the x-ray structural analysis. Therefore, the diffractograms of the surface were processed after cleaning the surface with sandpaper up to 15 μm . After replacing the substrate made of steel 40 with the one made of steel 20, a smaller amount of f.c.c. phase, namely the residual austenite, is found in the S-Mo coating at the same discharge energy, as shown in Fig. 38. Molybdenum disulphide is formed already at discharge energy of $W_p = 0.55$ J (3.77%), and $W_p = 3.4$ J; about 8% of it appears on the surface and about 5% of the same, at a depth of up to 15 μm in Table 19.

Thus, the process of sulphomolibdenizing the metal surfaces, which consists of applying a consistent substance containing sulphur and electrospark alloying thereof with a molybdenum electrode at discharge energies of 0.13, 0.55, and 3.4 J was investigated. Metallographic and durometric studies have shown that the sulphomolibdenized coatings consist of 4 zones: the upper loose layer having a microhardness of $H_\mu = 1112$ –2040 MPa, a white strengthened layer having $H_\mu = 5147$ –5474 MPa for $W_p = 0,13$ J and $H_\mu = 10596$ –10731 MPa for $W_p = 3.4$ J, a diffusion zone and a base metal. At replacing the substrate made of steel 20 by the one made of steel 40, there is an increase in the microhardness, the thickness of the strengthened layer, as well as in the continuity.

The electron microscopic studies of the obtained coatings have shown that the obtained layer has a heterogeneous composition with different concentrations of elements. According to the maps of the distribution of elements over the area of the specimens being studied, sulphur is concentrated on the surface; molybdenum is distributed more evenly in the coating. The energy dispersive analysis has shown that sulphur and molybdenum are concentrated at a depth of up to 4 and 19 μm , respectively, at $W_p = 0.13$ J; up to 5 and 25 μm at $W_p = 0.55$ J; up to 15 and 70 μm at $W_p = 3, 4$ J, respectively.

The x-ray structural analysis of the obtained coatings confirms the results of energy dispersion analysis. At low discharge energies, the phase composition of the coatings on steel 40 is represented by a bcc solid solu-

tion with a lattice period close to ferrite, by martensite, an f.c.c. solid solution, and FeMo intermetallic (σ -phase).

At replacing the substrate made of steel 40 with the one made of steel 20, a smaller amount of f.c.c. phase, namely the residual austenite, is found in the sulphomolibdenized coating at the same discharge energies. Molybdenum disulphide is formed already at discharge energy of $W_p = 0.55$ J (3.77%), and at $W_p = 3.4$ J, about 8% of it is found on the surface, and about 5% of the same is at a depth of up to 15 μm .

4. Conclusions

(i) Technologies for saturating metal surfaces with sulphur to provide them with tribological properties are here considered. Based on the results of a literature and patent search, an analysis of methods for sulphurizing by electrospark alloying is represented. It is shown that the process for saturating with sulphur can be implemented using STS containing sulphur. When the surface of steel 20 is saturated with sulphur by the ESA method using STS at the discharge energy $W_p = 0.55$ J, the concentration of sulphur on the surface is 0.53 to 0.60%. As the penetration increases, the concentration of sulphur has been gradually decreasing, and at a distance of 75 μm , it is about 0.06%. Therefore, the ESA method with the application of the STS can be used to process the friction pairs to eliminate seizure thereof.

(ii) The analysis of the quality parameters of the sulphocarbided coatings obtained by the energy-efficient and environmentally friendly ESA method with the use of the STS was carried out. According to the results of the analysis of the topography of the surface layer after sulphocarbiding by the ESA method, there has been established the uniform character of the shape of the formed elements of the surface micro-roughness. A significant increase in the micro-roughness amount on the surface of the specimens is observed with an increase in the discharge energy up to $W_p = 3.4$ J. In this case, the surface roughness is $R_a = 2.5$ μm . The metallographic and durometric analyses have shown that the treated surface consists of such layers as a co-called soft layer, a strengthened layer and a base metal. At increasing the discharge energy, the thickness, microhardness, and continuity of the coating have been increasing. The availability of sulphur in the STS promotes the sulphurizing process. As the discharge energy increases from 0.13 to 3.4 J at ESA processing steel 20, the amount of sulphur on the surface of the coating has been decreasing, but the thickness of the sulphurized layer has been increasing. The results of the micro-x-ray spectral analysis of the coatings indicate that the surface layers at a depth of 10 to 40 μm , depending on the energy parameters of the process, are saturated with sulphur. The sulphur concentration at this distance is about 0.4%. This zone is a layer of reduced microhardness.

A strengthened layer is formed under this layer. It is characterized by high carbon content and a high microhardness. The thickness of the strengthened layer depends on the energy parameters of the ESA process and is of 15 to 40 μm .

(iii) The analysis of the qualitative parameters of the sulphoaluminized coatings obtained by the EIL method with the use of the STS was carried out. The study of the surface profiles of the specimens after the ESA process and the roughness parameters of the surfaces being studied has shown that with an increase in W_p , as well as in the carbon content in the steel, the parameters R_a , R_z , R_{max} have been increasing. The metallographic and durometric analyses of the obtained coatings on steel 20 indicate that the three zones can be distinguished on the microstructures. Those are as follows: the near-surface zone, namely, a non-continuous loose layer of 10 to 100 μm thick and of a microhardness of 1368 to 2073 MPa, a white strengthened layer of 20 to 40 μm thick and of a microhardness of 4094 to 5157 MPa, a diffusion zone and a base metal having a ferrite-pearlite structure. At increasing W_p , the parameters of the layer, that is thickness, microhardness of the upper and white layers, as well as their continuity, have been increasing. At replacing the substrate material by steel 40 while sulphoaluminizing process, the hardness of both the upper layer (1670 and 2240 MPa at $W_p = 0.13$ and 3.4 J, respectively) and the strengthened layer (5147 and 10380 MPa at $W_p = 0.13$ and 3.4 J, respectively) have been increasing. The local micro-x-ray spectral analysis of the sulphoaluminized coatings has shown that the largest amount of sulphur is in the surface layer, which characterizes this layer as a layer of the decreased microhardness. In this case, sulphur is distributed over a depth of up to 10 microns. The diffusion zone of aluminium is of 30 to 80 μm , depending on the energy parameters of the ESA process. The highest aluminium content is typical for areas of the coating located at a distance of 7 to 15 μm from the surface. The near-surface soft layer is enriched with sulphur and strengthened with aluminium. The phase composition of sulphoaluminized coatings depends on the energy parameters of the ESA process, as well as on the carbon content in the base material. The FeAl intermetallic is formed in the surface layer. With an increase in W_p , there an intermetallic FeAl₂ is formed. In addition, a bcc solid solution is found in steel 20. In steel 40, at $W_p = 0.13$ J and at $W_p = 0.55$ J, an f.c.c. solid solution is created, and at $W_p = 3.4$ J, there is a bcc solid solution.

(iv) The special features of structure formation of Al-C-S coatings obtained by the ESA method with the use of STS were investigated. With a significant increase in the discharge energy (from 0.52 to 6.8 J), there is an increase in surface roughness and a decrease in the continuity of the coating. Microstructural analysis of Al-C-S coatings on steel 20 showed that the continuity and thickness of the white layer is 50% and 60 μm , respectively (at $W_p = 6.8$ J). In turn, the microhardness on the surface is

9000 MPa. The presence of sulphur in the STS contributes to the sulphurizing process: the amount of sulphur is maximal on the surface and it has been decreasing with distance from the surface.

(v). There has been an investigation of the process of sulphomolibdenizing the metal surfaces with the use of the STS in the course of the ESA. The metallographic and durometric studies have shown that the sulphomolibdenized coatings consist of 4 zones. Those are as follows: the upper loose layer with the microhardness of $H_{\mu} = 1112\text{--}2040$ MPa, the white strengthened layer with $H_{\mu} = 5147\text{--}5474$ MPa for $W_p = 0.13$ J and $H_{\mu} = 10596\text{--}10731$ MPa for $W_p = 3.4$ J, the diffusion zone, and the base metal. At replacing the substrate made of steel 20 by the substrate of steel 40, there is an increase in microhardness, the thickness of the strengthened layer, as well as in the continuity. Electron microscopic studies of the obtained coatings have shown that the obtained layer has a heterogeneous composition with different concentrations of elements. According to the maps of the distribution of the elements over the areas of the specimens being studied, sulphur is concentrated on the surface; molybdenum is distributed more evenly in the coating. The energy dispersive analysis has shown that sulphur and molybdenum are concentrated at a depth of up to 4 and 19 μm , respectively, at $W_p = 0.13$ J; up to 5 and 25 μm at $W_p = 0.55$ J; up to 15 and 70 μm at $W_p = 3, 4$ J, respectively. The x-ray structural analysis of the obtained coatings confirms the results of energy dispersion analysis.

At low discharge energies, the phase composition of coatings on steel 40 is represented by a bcc solid solution, with a lattice period similar to ferrite, martensite, f.c.c. solid solution and FeMo intermetallic (σ phase).

At replacing the substrate made of steel 40 by the one made of steel 20, a smaller amount of f.c.c. phase, namely, residual austenite has been found in the sulphomolibdenized coating at the same discharge energy. Molybdenum disulphide is formed already at a discharge energy of $W_p = 0.55$ J (3.77%), and at $W_p = 3.4$ J, about 8% thereof is found on the surface, and about 5% of the same is found at a depth of up to 15 μm .

Acknowledgement. Some of the results have been obtained within the research project ‘Development of environmentally safe technologies for surface modification of power plant equipment parts using combined methods based on electrospark alloying’ (State Reg. No. 0124U000539), Sumy State University, funded by the Ministry of Education and Science of Ukraine.

REFERENCES

1. A. Korczak, V. Martsynkovskyy, G. Peczkis, and A. Zahorulko, *Procedia Engineering*, **39**: 286 (2012);
<https://doi.org/10.1016/j.proeng.2012.07.035>
2. V. Martsynkovskyy, V. Tarelnyk, V. Martsynkovskyy, Ie. Konoplianchenko, A. Zhukov, P. Kurp, P. Furmańczyk, and N. Tarelnyk, *AIP Conf. Proc.*, **2017**: 020017 (2018);
<https://doi.org/10.1063/1.5056280>
3. V. Tarelnyk, I. Konoplianchenko, V. Martsynkovskyy, A. Zhukov, and P. Kurp, *Simulation and Manufacturing. DSMIE-2018. Lecture Notes in Mechanical Engineering* (Eds. V. Ivanov, Y. Rong, J. Trojanowska, J. Venus, O. Liaposhchenko, J. Zajac, I. Pavlenko, M. Edl, and D. Perakovic) (Cham: Springer: 2019), p. 382;
https://doi.org/10.1007/978-3-319-93587-4_40
4. V.B. Tarel'nik, V.S. Martsinkovskii, and A.N. Zhukov, *Chemical and Petroleum Engineering*, **53**, Nos. 1–2: 114 (2017);
<https://doi.org/10.1007/s10556-017-0305-y>
5. V.B. Tarel'nik, V.S. Martsinkovskii, and A.N. Zhukov, *Chemical Petroleum Engineering*, **53**, Nos. 3–4: 266 (2017);
<https://doi.org/10.1007/s10556-017-0333-7>
6. V.B. Tarel'nik, V.S. Martsinkovskii, and A.N. Zhukov, *Chemical Petroleum Engineering*, **53**, Nos. 5–6: 385 (2017);
<https://doi.org/10.1007/s10556-017-0351-5>
7. V.B. Tarelnyk, O.P. Gaponova, Ye.V. Konoplianchenko, V.S. Martsynkovskyy, N.V. Tarelnyk, and O.O. Vasylenko, *Metallofiz. Noveishie Tekhnol.*, **41**, No. 2: 173 (2019) (in Russian);
<https://doi.org/10.15407/mfint.41.02.0173>
8. T.V. Mosina, *Novyye Ogneupory*, **9**: 61 (2013);
<https://doi.org/10.17073/1683-4518-2013-9-61-64>
9. P. Rohatgi, M. Bellah, and V. Srivastava, *J. Mater. Res.*, **39**: 1597 (2024);
<https://doi.org/10.1557/s43578-024-01355-z>
10. A. Zahorulko, C. Kundera, and S. Hudkov, *IOP Conf. Ser. Mater. Sci. Eng.*, **233**: 012039 (2017);
<https://doi.org/10.1088/1757-899X/233/1/012039>
11. I.P. Shatskyi, V.V. Perepichka, and L.Ya. Ropyak, *Metallofiz. Noveishie Tekhnol.*, **42**, No. 1: 69 (2020) (in Ukrainian);
<https://doi.org/10.15407/mfint.42.01.0069>
12. O.P. Umanskyi, M.S. Storozhenko, V.B. Tarelnyk, N.V. Tarelnyk, and T.V. Kurinna, *Powder Metall. Met. Ceram.*, **59**, Nos. 1–2: 57 (2020);
<https://doi.org/10.1007/s11106-020-00138-5>
13. O. Umanskyi, M. Storozhenko, G. Baglyuk, O. Melnyk, V. Brazhevsky, O. Chernyshov, O. Terentiev, Yu. Gubin, O. Kostenko, and I. Martsenyuk, *Powder Metall. Met. Ceram.*, **59**, Nos. 7–8: 434 (2020);
<https://doi.org/10.1007/s11106-020-00177-y>
14. M. Bembenek, P. Prysyazhnyuk, T. Shihab, R. Machnik, O. Ivanov, and L. Ropyak, *Materials*, **15**, No. 14: 5074 (2022);
<https://doi.org/10.3390/ma15145074>
15. B.O. Trembach, M.G. Sukov, V.A. Vynar, I.O. Trembach, V.V. Subbotina, O.Yu. Rebrov, O.M. Rebrova, and V.I. Zakiev, *Metallofiz. Noveishie Tekhnol.*, **44**, No. 4: 493 (2022);
<https://doi.org/10.15407/mfint.44.04.0493>
16. H. Ichou, N. Arrousse, E. Berdimurodov, and N. Aliev, *J. Bio Tribo Corros.*, **10**: 3 (2024);
<https://doi.org/10.1007/s40735-023-00806-0>

17. E. Locks, Q. He, J.M. DePaiva, M. Guimaraes, A.F. Arif, S.C. Veldhuis, and J.R. Kish, *Coatings*, **14**, No. 3: 290 (2024);
<https://doi.org/10.3390/coatings14030290>
18. D.S. Rickerby and A. Matthews, *Advanced Surface Coatings: a Handbook of Surface Engineering* (Glasgow–Blackie–New York: Chapman and Hal: 1991).
19. D. Zhang, D. Du, Z. Pu, S. Xue, J. Qi, and B. Chang, *Materials Letters*, **363**: 136275 (2024);
<https://doi.org/10.1016/j.matlet.2024.136275>
20. B. Xu, P. Jiang, S. Geng, Y. Wang, J. Zhao, and G. Mi, *Materials & Design*, **203**: 109538 (2021);
<https://doi.org/10.1016/j.matdes.2021.109538>
21. P. Augustyn, P. Rytlewski, K. Moraczewski, and Adam Mazurkiewicz, *J. Mater. Sci.*, **56**: 14881 (2021);
<https://doi.org/10.1007/s10853-021-06246-w>
22. L. Sun, G. Yuan, L. Gao, J. Yang, M. Chhowalla, M.H. Gharahcheshmeh, K.K. Gleason, Y.S. Choi, B.H. Hong, and Z. Liu, *Nat. Rev. Methods Primers*, **1**: 5 (2021);
<https://doi.org/10.1038/s43586-020-00005-y>
23. L. Ropyak, I. Schuliar, and O. Bohachenko, *East-Eur. J. Ent. Technol.*, **1**, No. 5: 53 (2016) (in Ukrainian);
<https://doi.org/10.15587/1729-4061.2016.59850>
24. I. Ivashenko, V. Posuvailo, H. Veselivska, and V. Vynar, *Int. Sci. Tech. Conf. on Computer Sciences and Information Technologies*, **2**: 9321900 (2020);
<https://doi.org/10.1109/CSIT49958.2020.9321900>
25. M. Bembenek, M. Makoviichuk, I. Shatskyi, L. Ropyak, I. Pritula, L. Gryn, and V. Belyakovskiy, *Sensors*, **22**, No. 21: 8105 (2022);
<https://doi.org/10.3390/s22218105>
26. M.M. Student, V.M. Dovhunyk, V.M., Posuvailo, I.V. Koval'chuk, and V.M. Hvozdet'skyi, *Mater. Sci.*, **53**, No. 3: 359 (2017);
<https://doi.org/10.1007/s11003-017-0083-x>
27. O. Bazaluk, O. Dubei, L. Ropyak, M. Shovkopliias, T. Pryhorovska, and V. Lozynskiy, *Energies*, **15**, No. 1: 83, (2022);
<https://doi.org/10.3390/en15010083>
28. T. Loskutova, M.Scheffler, V. Ivanov, I. Pohrebova, Y. Kononenko, M. Bobina, N. Kharchenko, M. Bartoszuk, and I. Pavlenko, *Metals*, **14**, No. 3: 302 (2024);
<https://doi.org/10.3390/met14030302>
29. S. Yeh, L. Chiu, and H. Chang, *Eng. Sci. Res. Publ.*, **9**, No. 3: 942 (2011);
<https://doi.org/10.4236/eng.2011.39116>
30. S. Ben Slima, *Mater. Sci. Appl. Sci. Res. Publ.*, **9**, No. 3: 640 (2012);
<https://doi.org/10.4236/msa.2012.39093>
31. M. Stoicescu, E. Ene, A. Zara, I. Giacomelli, and A.C. Berbecaru, *U.P.B. Sci. Bull. Ser. B.*, **80**, No. 4: 157 (2018);
32. L.A. Harlamov and O.S. Kroli, *Volodymyr Dal National University of Eastern Ukraine* (Donetsk: 2015), p. 223.
33. M. Nikolova, N. Nikolov, E. Yankov, B. Derin, and S. Topalski, *Indian J. Eng. Mater. Sci.*, **27**, No. 14: 5 (2020);
<https://doi.org/10.56042/ijems.v27i1.45867>
34. W. Hai-dou, Z. Da-ming, W. Kun-lin, and L. Jia-jun, *Mater. Sci. Eng.*, **357**, Nos. 1–2: 321 (2003);
[https://doi.org/10.1016/S0921-5093\(03\)00209-0](https://doi.org/10.1016/S0921-5093(03)00209-0)
35. J.J. Kang, C.B. Wang, H.D. Wang, B.S. Xu, J.J. Liu, and G.L. Li, *Adv. Mater. Res.*, **217–218**: 1117 (2011);

- <https://doi.org/10.4028/www.scientific.net/AMR.217-218.1117>
36. J.J. Kang, C.B. Wang, H.D. Wang, B.S. Xu, J.J. Liu, and G.L. Li, *Adv. Mater. Res.*, **217–218**: 1113 (2011);
<https://doi.org/10.4028/www.scientific.net/AMR.217-218.1113>
37. J.J. Kang, C.B. Wang, H.D. Wang, B.S. Xu, J.J. Liu, and G.L. Li, *Mater. Chem. Phys.*, **129**, Nos. 1–2: 625 (2011);
<https://doi.org/10.1016/j.matchemphys.2011.05.002>
38. J.J. Kang, C.B. Wang, H.D. Wang, B.S. Xu, J.J. Liu, and G.L. Li, *Surf. Coat. Technol.*, **203**, No. 14: 1927 (2009);
<https://doi.org/10.1016/j.surfcoat.2009.01.017>
39. N. Zhang, D.M. Zhuang, and J.J. Liu, *Surf. Coat. Technol.*, **203**, No. 20: 3173 (2009);
<https://doi.org/10.1016/j.surfcoat.2009.03.046>
40. H.D. Wang, B.S. Xu, J.J. Liu, D.M. Zhuang, S.C. Wei, and G. Jin, *Surf. Coat. Technol.*, **201**, Nos. 9–11: 5286 (2007);
<https://doi.org/10.1016/j.surfcoat.2006.07.229>
41. H.D. Wang, B.S. Xu, J.J. Liu, and D.M. Zhuang, *Surf. Coat. Technol.*, **201**, Nos. 9–11: 5236 (2007);
<https://doi.org/10.1016/j.surfcoat.2006.07.226>
42. V.I. Kuzmin, A.A. Mikhal'chenko, O.B. Kovalev, and N.A. Rudenskaya, *J. Thermal Spray Technology*, **21**, No. 1: 159 (2012);
<https://doi.org/10.1007/s11666-011-9701-6>
43. A.D. Pogrebnyak, V.I. Ivashchenko, P.L. Skrynskyy, O.V. Bondar, P. Konarski, K. Zaleski, S. Jurga, and E. Coy, *Composites. Part B: Eng.*, **142**: 85 (2018);
<https://doi.org/10.1016/j.compositesb.2018.01.004>
44. A.D. Pogrebnyak, A.A. Bagdasaryan, P. Horodek, V. Tarelnyk, V.V. Buranich, H. Amekura, N. Okubo, N. Ishikawa, and V.M. Beresnev, *Materials Letters*, **303**, 130548 (2021);
<https://doi.org/10.1016/j.matlet.2021.130548>
45. G. Morand, P. Chevallier, L. Bonilla-Gameros, S. Turgeon, M. Cloutier, M. Da Silva Pires, A. Sarkissian, M. Tatoulian, L. Houssiau, and D. Mantovani, *Surf. Interface Analysis*, **53**, No. 7: 658 (2021);
<https://doi.org/10.1002/sia.6953>
46. G. Maistro, S. Kante, L. Nyborg, and Y. Cao, *Surf. Interf.*, **24**: 101093 (2021);
<https://doi.org/10.1016/j.surfin.2021.101093>
47. B. Antoszewski, S. Tofil, M. Scendo, and W. Tarelnik, *IOP Conf. Ser.: Mater. Sci. Eng.*, **233**: 012036 (2017);
<https://doi.org/10.1088/1757-899X/233/1/012036>
48. B. Antoszewski, N. Radek, W. Tarelnik, and E. Wajs, *IX Int. Conf. HERVICON* (2005, Sumy), p. 15.
49. N. Radek, *Mechanik*, **83**, No. 11: 822 (2010).
50. J. Padgurskas, R. Kreivaitis, R. Rukuiza, V. Mihailov, V. Agafii, R. Kriūkienė, and A. Baltušnikas, *Surf. Coat. Technol.*, **311**: 90 (2017);
<https://doi.org/10.1016/j.surfcoat.2016.12.098>
51. M. Salmalian, F. Malek Ghaeni, and M. Ebrahimnia, *Surf. Coat. Technol.*, **321**: 81 (2017);
<https://doi.org/10.1016/j.surfcoat.2017.04.040>
52. H. Aghajani, E. Hadavand, N.S. Peighambardoust, and S. Khameneh-asl, *Surf. Interf.*, **18**, No. 4: 100392 (2020);
<https://doi.org/10.1016/j.surfin.2019.100392>
53. B. Antoszewski and V. Tarelnik, *Appl. Mech. Mater.*, **630**: 301 (2014);
<https://doi.org/10.4028/www.scientific.net/AMM.630.301>

54. A. Gadek-Moszczak, N. Radek, S. Wroński, and J. Tarasiuk, *Adv. Mater. Res.*, **874**: 133 (2014);
<http://dx.doi.org/10.4028/www.scientific.net/AMR.874.133>
55. N. Radek, J. Konstanty, and M. Scendo, *Arch. Metall. Mater.*, **60**, No. 4: 2579 (2015);
<https://doi.org/10.1515/amm-2015-0417>
56. V. Tarel'nyk, I. Konoplianchenko, O. Gaponova, N. Tarel'nyk, V. Martsynkovskyy, B. Sarzhanov, O. Sarzhanov, and B. Antoszewski, *Powder Metall. Met. Ceram.*, **58**: 703 (2020);
<https://doi.org/10.1007/s11106-020-00127-8>
57. B. Antoszewski, S. Tofill, M. Scendo, and W. Tarelnik, *IOP Conf. Ser.: Mater. Sci. Eng.*, **233**: 012036 (2017);
<https://doi.org/10.1088/1757-899X/233/1/012036>
58. O.M. Myslyvchenko, O.P. Gaponova, V.B. Tarel'nyk, and M.O. Krapivka, *Powder Metall. Metal. Ceram.*, **59**, Nos. 3–4: 201 (2020);
<https://doi.org/10.1007/s11106-020-00152-7>
59. V.B. Tarel'nyk, O.P. Gaponova, Ye.V. Konoplyanchenko, N. S. Yevtushenko, and V.O. Herasymenko, *Metallofiz. Noveishie Tekhnol.*, **40**, No. 6: 795 (2018) (in Russian);
<https://doi.org/10.15407/mfint.40.06.0795>
60. C. Barile, C. Casavola, G. Pappalettera, and G. Renna, *Coatings*, **12**, No. 10: 1536 (2022);
<https://doi.org/10.3390/coatings12101536>
61. J. Wang, M. Zhang, S. Dai, and L. Zhu, *Coatings*, **13**, No. 8: 1473 (2023);
<https://doi.org/10.3390/coatings13081473>
62. V.B. Tarel'nyk, O.P. Gaponova, V.B. Loboda, E.V. Konoplyanchenko, V.S. Martsinkovskii, Yu.I. Semirnenko, N.V. Tarel'nyk, M.A. Mikulina, and B.A. Sarzhanov, *Engin. Appl. Electrochem.*, **57**: 173 (2021);
<https://doi.org/10.3103/S1068375521020113>
63. V.B. Tarel'nyk, A.V. Paustovskii, Y.G. Tkachenko, E.V. Konoplianchenko, V.S. Martsynkovskiy, and B. Antoszewski, *Powder Metall. Met.. Ceram.*, **55**: 585 (2017);
<https://doi.org/10.1007/s11106-017-9843-2>
64. V. Martsynkovskyy, V. Tarel'nyk, I. Konoplianchenko, O. Gaponova, and M. Dumanchuk, *Advances in Design, Simulation and Manufacturing II. DSMIE 2019. Lecture Notes in Mechanical Engineering* (Eds. V. Ivanov, Y. Rong, J. Trojanowska, J. Venus, O. Liaposhchenko, J. Zajac, I. Pavlenko, M. Edl, D. Perakovic (Cham: Springer: 2020);
https://doi.org/10.1007/978-3-030-22365-6_22
65. V.B. Tarel'nik, A.V. Paustovskii, Y.G. Tkachenko, V.S. Martsinkovskii, E.V. Konoplyanchenko, and K. Antoshevskii, *Surf. Eng. Appl. Electrochem.*, **53**, No. 3: 285 (2017);
<https://doi.org/10.3103/S1068375517030140>
66. A.A. Ishchenko, *Tekhnologichni Osnovy Vidnovlennya Promyslovoho Obladnannya Suchasnyy Polimernyy Materialamy* [Technological Foundations of Restoration of Industrial Equipment with Modern Polymeric Materials] (Mariupol: PDTU: 2007), p. 250 (in Ukrainian).
67. V.B. Tarel'nik, E.V. Konoplyanchenko, P.V. Kosenko, and V.S. Martsinkovskii, *Chem. Petrol. Eng.*, **53**, Nos. 7–8: 540 (2017);
<https://doi.org/10.1007/s10556-017-0378-7>
68. V. Martsinkovsky, V. Yurko, V. Tarelnik, and Yu. Filonenko, *Procedia Engineering*, **39**: 148 (2012);
<https://doi.org/10.1016/j.proeng.2012.07.019>

69. V. Martsinkovsky, V. Yurko, V. Tarelnik, and Yu. Filonenko, *Procedia Eng.*, **39**: 157 (2012);
<https://doi.org/10.1016/j.proeng.2012.07.020>
70. C.A. da Silva, J.A. Moreto, D.V. de Castro, and H.de Araújo Ponte, *J. ASTM Int.*, **9**, No. 1: 1 (2011);
<https://doi.org/10.1520/JAI103398>
71. G. Zhang, J. Ouyang, X. Meng, L. Ma, Q. Shangkui, and F. Zhang, *Wear*, **162–164**, Pt. A: 450 (1993);
[https://doi.org/10.1016/0043-1648\(93\)90529-U](https://doi.org/10.1016/0043-1648(93)90529-U)
72. N.I. Lazarenko, *Ehlektroiskrovoye Legirovanie Metallicheskih Poverkhnostei* [Electric Spark Alloying of Metal Surfaces] (Moskva: Mashinostroenie: 1976), p. 46 (in Russian).
73. A.G. Shcherbinskii, *Sposob Nasyshcheniya Poverkhnostei Metalla Seroi* [Method of Saturating Metal Surfaces with Sulphur]: *Patent 139336 RU*. (1961) (in Russian).
74. V. Tarelnyk, V. Martsynkovskyy, O. Gaponova, N. Tarelnyk, and S. Gorovoy, *IOP Conf. Ser.: Mater. Sci. Eng.*, **233**, No. 1: 012049 (2017);
<https://doi.org/10.1088/1757-899X/233/1/012049>
75. V.B. Tarelnik, V.S. Martsinkovskii, and B. Antoshevskii, *Kompressornoe i Energeticheskoe Mashinostroenie*, **4**, No. 6: 66 (2006) (in Russian).
76. V. Tarelnyk, I. Konoplianchenko, O. Gaponova, N. Tarelnyk, V. Martsynkovskyy, B. Sarzhanov, O. Sarzhanov, and B. Antoszewski, *Powder Metall. Met. Ceram.*, **58**: 703 (2020);
<https://doi.org/10.1007/s11106-020-00127-8>
77. F. Georgee, *Vander Applied Metallography* (New York: Springer Science & Business Media: 2012).
78. *GOST 9450-76. Izmerenie Mikrotverdosti Metodom Vdavlivaniya Almaznykh Nakhonechnikov* [Microhardness Measurement by Diamond Tip Indentation Method] (Moskva: Izd-vo Standartov: 1978), p. 56 (in Russian).
79. *DSTU ISO 6507-1:2007. Materialy Metalevi. Vyznachennya Tverdosti za Vikersom. Ch. 1. Metod Vyprobuvannya (ISO 6507-1:2005, IDT)* [Metal Materials. The Hardness Value Determined by Vickers. Pt. 1. Testing Method] (Kyiv: Derzhspozhyvstandart Ukrainy: 2010), p. 20 (in Ukrainian).
80. *GOST 1778-70. Stal. Metallograficheskie Metodi Opredeleniya Nemetallicheskikh Vkhlyuchenii* [Steel. Metallographic Methods for Determining Non-Metallic Inclusions] (Standartinform: 2011), p. 32 (in Russian).
81. V.B. Tarelnyk, O.P. Gaponova, Ye.V. Konoplianchenko, V.S. Martsynkovskyy, N.V. Tarelnyk, and O.O. Vasylenko, *Metallofiz. Noveishie Tekhnol.*, **41**, No. 2: 173 (2019) (in Russian);
<https://doi.org/10.15407/mfint.41.02.0173>
82. V.B. Tarelnyk, V.S. Martsynkovskyy, A.V. Bilous, O.M. Zhukov, P.V. Kosenko, and O.P. Haponova, *Sposib Sulfiduvannya Poverkhni Stalevykh i Chavunnykh Detalei Metod Elektroeroziinogo Leguvannya* [The Method of Sulphiding the Surface of Steel and Cast Iron Parts by Electroerosion Alloying]: Patent 115059 RU, IPC (2017.01), B23H 1/00, C23C 8/60 (2006.01), C22C 37/00, C22C 37/06, C22C 37/08 (Bul. 6) (2017) (in Ukrainian).
83. V.B. Tarelnyk, V.S. Martsynkovskyy, A.V. Bilous, O.P. Haponova, Ye.V. Konoplianchenko, B. Antoshevskyy, Ch. Kundera, and O.M. Zhukov, *Sposib Nasyshcheniya Poverkhni Stalevykh i Chavunnykh Detalei Sirkoyu Metod Elektroeroziinogo Leguvannya* [The Method of Saturating the Surface of Steel and Cast Iron Parts with Sulphur by Electroerosion Alloying]: Patent 119317 UA, IPC (2017.01), B23H 1/00, C23C 8/60 (2006.01) (Bul. 18) (2017) (in Ukrainian).

84. V.B. Tarelnyk, V.S. Martsynkovskiyi, A.V. Bilous, O.M. Zhukov, O.P. Haponova, and Ye.V. Konoplianchenko, *Sposib Sulfotsementatsii Poverkhni Stalevoi Detali* [The Method of Sulfocementation of the Surface of a Steel Part]: Patent 117867 UA, IPC B23H 1/00 B23H 9/02, C23C 8/66 (2006.01) (Bul.19) (2018) (in Ukrainian).
85. O.P. Gaponova, V.B. Tarelnyk, N.V. Tarelnyk, and P. Kurp, *Solid State Phenomena*, **355**: 85 (2024);
<https://doi.org/10.4028/p-5KfyZQ>
86. V.B. Tarelnyk, V.S. Martsynkovskiyi, A.V. Bilous, O.P.Haponova, Ye.V. Konoplianchenko, B. Antoshevskiyi, Ch. Kundera, and O.M. Zhukov, *Sposib Sulfotsementatsii Stalevykh Detalei* [The Method of Sulfocementation of Steel Parts]: Patent 119318 UA, IPC (2017.01), B23H 1/00, B23H 9/00, C23C 8/60 (2006.01) (Bul. 22) (2017) (in Ukrainian).
87. B. Antoszewski, O.P. Gaponova, V.B. Tarelnyk, O.M. Myslyvchenko, P. Kurp, T.I. Zhylenko, and I. Konoplianchenko, *Materials*, **14**: 739 (2021);
<https://doi.org/10.3390/ma14040739>
88. O.P. Haponova, *Visnyk Kharkivskoho Natsionalnogo Tekhnichnogo Universytetu Silskogo Gospodarstva imeni Petra Vasylenka. Problemy Nadiinosti Mashyn*, **205**: 339 (2019) (in Ukrainian).
89. L.D. Plyatsuk, V.B. Tarelnyk, Cz. Kundera, O.V. Radionov, and O.P. Gaponova, *J. Eng. Sci.*, **5**, No. 1: 16 (2018);
[https://doi.org/10.21272/jes.2018.5\(1\).c4](https://doi.org/10.21272/jes.2018.5(1).c4)
90. V.B. Tarelnyk, V.S. Martsynkovskiyi, A.V. Belous, A.N. Zhukov, O.P. Haponova, and E.V. Konoplianchenko, *Sposob Sulfotsementatsii Stalnykh Detalei* [The Method of Sulfocementation of Steel Parts]: Patent 2663799 RU, IPC B23H 1/00 (2006.01), B2H 9/00 (2006.01) (Bul. 22) (2018) (in Russian).
91. S.N. Himuhin, H. Ri, and E.X. Ri, *Struktura i Svoystva Metallov i Splavov pri Elektroiskrovom Vozdeystvii* [Structure and Properties of Metals and Alloys under Electric Spark Action] (Khabarovsk: Tikhookeanskiy Gos. Univer.: 2015) (in Russian).
92. G.V. Kirik, O.P. Gaponova, V.B. Tarelnyk O.M. Myslyvchenko, and B. Antoszewski, *Powder Metallurgy and Metal Ceramics.*, **56**, Nos. 11–12: 688 (2018);
<https://doi.org/10.1007/s11106-018-9944-6>
93. O. Gaponova, C. Kundera, G. Kirik V. Tarelnyk, V. Martsynkovskyy, Ie. Konoplianchenko, M. Dovzhyk, A. Belous, and O. Vasilenko, *Advances in Thin Films, Nanostructured Materials, and Coatings. NAP 2018. Lecture Notes in Mechanical Engineering* (Singapore: Springer: 2019), p. 249;
https://doi.org/10.1007/978-981-13-6133-3_25
94. V. Tarelnyk, V. Martsynkovskyy, O. Gaponova, Ie. Konoplianchenko, A. Belous, V. Gerasimenko, and M. Zakharov, *15th Int. Sci. Eng. Conf. Hermetic Sealing, Vibration Reliability and Ecological Safety of Pump and Compressor Machinery, HERVICON+PUMPS*, **233**, No. 1: 012048 (2017);
<https://doi.org/10.1088/1757-899X/233/1/012048>
95. A. Cowley and B. Mintz, *Mater. Sci. Technol.*, **20**, No. 11: 1431 (2004);
<https://doi.org/10.1179/026708304X4268>
96. V.B. Tarelnyk, V.S. Martsynkovskiyi, O.P. Gaponova, Ye. Konoplianchenko, N.V. Tarelnyk, M.Yu. Dumanchuk, M.V. Honcharenko, B. Antoshevskiyi, and Ch. Kundera, *Sposib Obrobky Poverkhon Stalevykh Detalei* [The Method of Processing the Surfaces of Steel Parts]: Patent 121346 UA. IPC B23H 1/06 (2006.01), B23H 9/00, C23C 12/02 (2006.01) (Bul. 9) (2020) (in Ukrainian).

97. V.B. Tarelnyk, O.P. Gaponova, and Ye.V. Konoplianchenko, *Progress in Physics of Metals*, **23**, No. 1: 27 (2022);
<https://doi.org/10.15407/ufm.23.01.027>
98. V.B. Tarelnyk, E.V. Konoplyanchenko, O.P. Gaponova, and N.V. Tarelnik, *Ensuring the Protection of the Surfaces of End Pulse Seals of Turbomachines by Forming Wear-Resistant Nanostructures* (Sumy: University Book: 2022).
99. R.N. Johnson, *45th Annual Technical Conf. Proceedings, Society of Vacuum Coaters (April 13–18, 2002, Madison, MI, USA)*, p. 87.
100. J.L. Reynold, R.L. Holdren, and L.E. Brown, *Adv. Mater. Process.*, **161**, No. 3: 35 (2003).
101. R. Johnson and G. Sheldon, *J. Vac. Sci. Technol. A*, **4**, No. 6: 2740 (1986);
<https://doi.org/10.1116/1.573672>
102. O.P. Gaponova, B. Antoszewski, V.B. Tarelnyk, O.M. Myslyvchenko, and N.V. Tarelnyk, *Materials*, **14**, No. 21: 63322021 (2021);
<https://doi.org/10.3390/ma14216332>
103. V.B. Tarelnyk, V.S. Martynkovskiy, O.P. Gaponova, O.M. Myslyvchenko, V.O. Pyrohov, O.O. Hapon, and A.D. Lazarenko, *Sposib Formuvannya Pokryttya na Poverkhni Stalevoi Detali Metodrom Ehlektroiskrovoho Leguvannya* [The Method of Forming the Coating on the Surface of a Steel Part by the Electric-Spark Alloying Method]: Patent 144932 UA. IPC B23H 1/00, B23H 9/00, C23C 4/00, C23C 6/00, C23C 8/60 (2006.01) (Bul. 21) (2020) (in Ukrainian).
104. O. Haponova, V. Tarelnyk, T. Mościcki, N. Tarelnyk, J. Pyrolniczak, O. Myslyvchenko, B. Adamczyk-Cieślak, and J. Sulej-Chojnacka, *Coatings*, **14**: 563 (2024);
<https://doi.org/10.3390/coatings14050563>

Received 14.08.2024
Final version 03.02.2025

В.В. Тарельник¹, О.П. Гапонова^{2,3}, Н.В. Тарельник¹, Є.В. Конопляченко¹

¹ Сумський національний аграрний університет,
вул. Г. Кондратьєва, 160, 40021 Суми, Україна

² Сумський державний університет,
вул. Харківська, 116, 40007 Суми, Україна

³ Інститут фундаментальних технологічних досліджень
Польської академії наук,
вул. Павіньського, 5Б, 02-016 Варшава, Польща

СУЛЬФІДУВАННЯ МЕТАЛЕВИХ ПОВЕРХОНЬ ЕЛЕКТРОІСКРОВИМ ЛЕГУВАННЯМ.

Ч. 1: Структурно-фазовий стан сірковмісних покриттів на конструкційних сталях

Розглянуто та проаналізовано методи поверхневого насичення Сульфуром металевих поверхонь для надання їм спеціальних триботехнічних властивостей. Основну увагу зосереджено на технологіях, що ґрунтуються на методі електроіскрового легування (ЕІЛ). Показано, що процес насичення Сульфуром можна реалізувати, використовуючи спеціальні насичувальні середовища (СНС), що містять Сульфур. Розглянуто способи формування сульфідованого, сульфоцементованого, сульфоалітованого, Al–C–S, сульфомолібденового покриттів на сталях за допомогою СНС методом ЕІЛ. Наведено результати розподілу Сульфур у поверхневому шарі під час сульфідкування ЕІЛ металевим електродом з використанням СНС. Показано, що концентрація Сульфур на поверхні становить близько 0,53–0,60 % і поступово зменшується вглиб підкладки. Досліджено топографію обробленої поверхні, її структуру після сульфоцементування сталевих поверхонь графітовим електродом з ви-

користанням СНС, що містить Сульфур. Встановлено, що покриття складається з кількох шарів: насиченого Сульфуром «м'якого», насиченого Карбоном зміцненого й основного металу. Зі зростанням енергії розряду збільшуються товщина, мікротвердість і суцільність покриття. Проаналізовано якісні параметри сульфоалітованих покриттів, одержаних методом ЕІЛ алюмінієвим електродом з використанням СНС. На мікроструктурах виявляються три зони: збагачений Сульфуром приповерхневий несцільний пухкий шар завтовшки у 10–100 мкм і мікротвердістю у 1368–2073 МПа, «білий» зміцнений шар завтовшки у 20–40 мкм і мікротвердістю у 4094–5157 МПа із вмістом Алюмінію, дифузійна зона та матеріал підкладки. Фазовий склад сульфоалітованих покриттів залежить від енергетичних параметрів ЕІЛ. У поверхневому шарі утворюються інтерметаліди $FeAl$ і $FeAl_2$. Досліджено структурно-фазовий стан і властивості сульфомолібденових покриттів, одержаних методом ЕІЛ молібденовим електродом з використанням СНС. Приповерхневий пухкий шар, насичений Сульфуром, містить до 8 % дисульфиду Молібдену, що утворився в результаті ЕІЛ. Під цим шаром міститься насичений Молібденом зміцнений шар мікротвердістю у 10596–10731 МПа. Методи сульфидування на основі ЕІЛ з використанням СНС запропоновано використовувати як дешеві й ефективні способи поверхневого модифікування поверхонь тертя для усунення заїдання та зменшення коефіцієнтів тертя.

Ключові слова: сульфидування, електроіскрове легування, покриття, мікроструктура, триботехнічні властивості.